transplanted with Cy5.5-labeled BM-MNCs obtained from ICR/EGFP mice is shown (left column). The cells from the tibiae were observed under an inverted fluorescent microscope (right column). Bar = 40 μm. Green, EGFP; blue, DAPI; red, Cy5.5. (D) FACS analysis of chimerism of Cy5.5 and EGFP double-positive cells in the tibiae at the indicated times.
doi:10.1371/journal.pone.0011114.g002

Evaluation of in vivo imaging of NIFR-labeled donor cells revealed that the NIRF tracking approach is highly sensitive

Next, we transplanted AF750-labeled ICR/EGFP BM-MNCs into the Balb/c nu/nu mice to evaluate the sensitivity and accuracy of our approach for tracking the homing process of donor cells in vivo. Distribution of the donor cells was monitored using an in vivo imaging device for 24 h after BMT. Using AF750-labeled cells, transplanted cells were detected in many organs in vivo (Fig. 3A). The distribution of donor cells was spread over several organs including the lung, liver, spleen, and BM (Fig. 3B). Ex vivo imaging of the recipient mice at 24 h after BMT confirmed NIRF signal distribution in the tissues suggested by in vivo imaging (Fig. 3C). Significant NIRF signals were detected in BM and the reticuloendothelial system, but not in the GI tract (Fig. 3C). To confirm the presence of donor cells in the tissues detected by ex vivo fluorescent imaging, sections of the tissues were examined for presence of $EGFP^+$ cells 24 h after transplantation (Fig. 3D). Although significant fluorescent signals were detected in the tissues by in vivo and ex vivo imaging, the $EGFP^+$ cells were sparsely distributed in each tissue, indicating that in vivo NIRF imaging is highly sensitive.

In vivo and ex vivo tracking of AF750-labeled cells in various congenic BMT models in an initial phase after transplantation

The above results strongly suggest that in vivo imaging of NIRF-labeled donor cells would provide a highly sensitive and accurate method to track the homing process of transplanted cells. First, congenic BMT was performed to evaluate the homing process of transplanted cells in the absence of rejection. Biodistributions of the transplanted BM-MNCs labeled with AF750 were then compared in various congenic BMT models at an early stage after transplantation. The AF750 images obtained after injection of NIRF-unlabeled BM-MNCs were identical to those of the background signals in PBS-injected mice (Supplemental Fig. S8). After intravenous injection of free AF750, the fluorescent signal disappeared through the urinary system within 1 h after BMT (Supplemental Fig. S8). In the congenic BMT model mice, the fluorescent signal was detectable in both tibiae 5 min after transplantation. It gradually increased by 3 h and remained unchanged for the rest of the observation period (Fig. 4A, supine position). We detected transplanted cell homing in vivo at 5 min after BMT, which is the earliest detection time reported thus far. In the reticuloendothelial system, the transplanted cells were first seen trapped in the lung 5 min after BMT and then in the liver and spleen 15 min after BMT. In the IBM-BMT model, the transplanted cells were seen trapped in the lung through the peripheral circulation 5 min after IBM-BMT (Fig. 4A, supine position). In this model, the donor cells migrated from the left tibia to the right one within 1 h after BMT (Fig. 4A, supine position), although many cells stayed in the left tibia for 24 h. Tissue distribution of the fluorescent signal was examined by ex vivo imaging 24 h after BMT in both BMT models. When the free AF750 dye was injected intravenously, the background level slightly increased in each organ, although the increase was negligible (Fig. 4B). In a comparison of congenic BMT with congenic IBM-BMT (Fig. 4B), most of the donor cells were found to remain in the injected left tibia in congenic IBM-BMT mice, while most of the donor cells migrated to all bones of the body in the congenic BMT mice. To our knowledge, this is the first report using in vivo imaging to reveal the distribution dynamics of transplanted cells after IBM-BMT, and the results suggest that the NIRF labeling approach would be applicable in various congenic BMT models.

Transplanted donor cell division starts more than 24 h after BMT

To determine the start time of transplanted donor cell division after homing, we harvested the cells from the tibiae and peripheral blood of the recipient mice at 24, 48, and 72 h after transplantation of AF750-labeled ICR/EGFP BM-MNCs and examined the fraction of $EGFP^+$ cells present by FACS (Fig. 5A). The NIRF intensity of $EGFP^+$ cells 24 h after BMT was similar to that of preBMT cells (Figs. 5A, B second row), indicating that the donor cells had not started cell division until then because NIRF intensity decreased with cell division (Fig. 1D, Supplemental Fig. S3). Donor cell division started thereafter because the chimerism of $EGFP^+$ cells in the tibiae of the recipients increased by approximately 45% at 72 h after BMT (Figs. 5B, C). FACS analysis revealed that the donor cell population contained all leukocyte fractions at 72 h after BMT (Fig. 5B, top right panel) and that $EGFP^+$ appeared in the peripheral blood at 72 h with similar fluorescence intensity as that in BM (Fig. 5D, Supplemental Fig. S9).

Immunohistochemical analysis confirmed that the number of transplanted $EGFP^+$ cells did not increase until 24 h after BMT and then rapidly expanded in the epiphyseal area of the tibia and femur between 48 and 72 h after BMT (Figs. 5E, F). These results indicate that transplanted donor cell division starts more than 24 h after BMT and that hematopoietic reconstitution in Balb/c nu/nu recipient mice begins approximately 72 h after BMT.

In vivo and ex vivo tracking of AF750-labeled cells in various allogeneic BMT models

We attempted to visualize the biodistribution of allogeneic BMT models with C57BL/6 (as donors) and Balb/c nu/nu mice (as recipients) to analyze the onset of aGVHD. Because the depletion of donor T cells abrogates GVHD [15], TCD-BMT (nonGVHD) and TCD-BMT plus Sp-MNCs (GVHD) transplantation models were established. In allogeneic BMT and the GVHD models, the fluorescent signals from the reticuloendothelial system were very high at 24 h after BMT (Fig. 6A, right top and bottom panels). The tissues with a high fluorescent signal were confirmed by ex vivo imaging 24 h after BMT (Fig. 6B). Among the reticuloendothelial system, the fluorescence was lowest in the nonGVHD model and highest in the GVHD model (Fig. 6B). These results indicate that the presence of a T-cell population in the donor cells causes homing to the reticuloendothelial system and that the TCD donor cells predominantly homed to BM. The fluorescent signal was very weak in the intestinal tract in all allogeneic BMT models (Fig. 6B, bottom row).

Discussion

To our knowledge, this study is the first report describing the use of in vivo real-time imaging to visualize the distribution dynamics of transplanted BM cells in the entire body during the

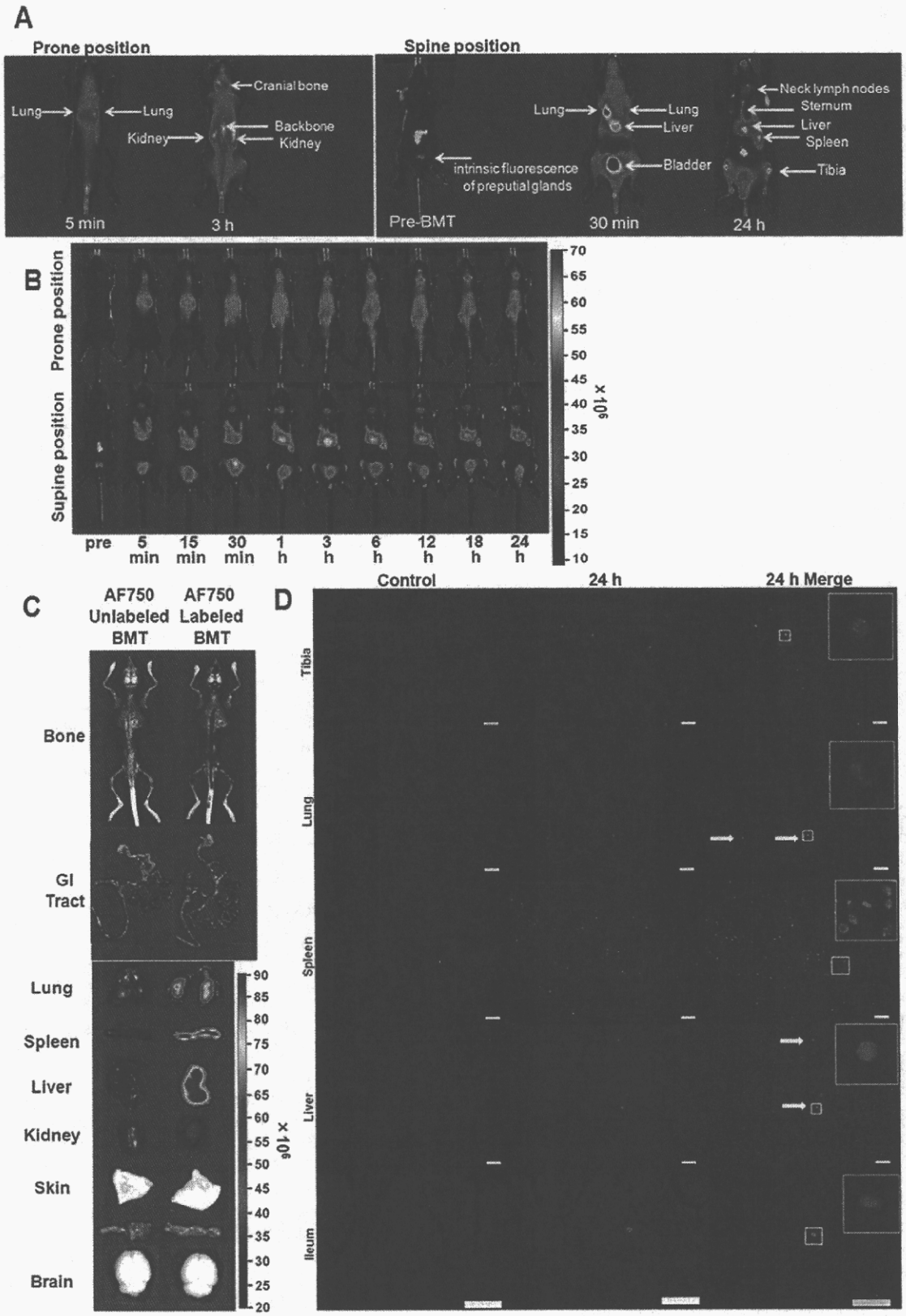

Figure 3. Fluorescent signals from AF750/EGFP double-positive cells were detected in vivo with extremely high sensitivity. Lethally irradiated Balb/c nu/nu (H-2^d) mice were transplanted with 1×10^7 AF750-labeled ICR/EGFP BM-MNCs. (A) Sources of NIRF signals in vivo. The congenic BMT model is shown as an example. (B) Representative in vivo images of the recipient mice at the indicated times after BMT. The prone (upper row) and supine (bottom row) positions are shown. (C) Ex vivo imaging of the recipient mice. Mice transplanted with AF750-labeled (left) or unlabeled (right) BM-MNCs were sacrificed at 24 h after BMT. The congenic AF750-unlabeled BMT model is shown as a control. (D) Fluorescence images of various organs from recipient mice. AF750-labeled ICR/EGFP BM-MNCs were transplanted, and the organs were examined 24 h after

BMT. Untreated Balb/c nu/nu mice were used as controls. Green, EGFP; blue, DAPI. White arrows show EGFP/DAPI double-positive cells. Bar = 100 μm.
doi:10.1371/journal.pone.0011114.g003

initial phase after BMT using the NIRF method. Achieving in vivo imaging at a very early stage after BMT was previously difficult because the small number of cells that escape the reticuloendothelial system result in minute cell distributions within each organ. In this study, we labeled the surface of transplanted cells with NIRF and successfully demonstrated the altered distribution dynamics of transplanted cells in the initial phase. We could noninvasively track transplanted cells circulating in the entire body during the initial stage after BMT because of the following reasons: (1) NIRF illumination with higher light propagation and lower attenuation through the tissue was used as both excitation and emission light for imaging [16]; (2) homogeneous labeling on the cell surface with NIRF dyes was achieved despite a variety of cell populations; (3) NIRF-labeled transplanted donor cells had a constant MFI, detectable in vivo over a 24-h period; (4) Balb/c nu/nu mice (hairless mice) were used to enhance NIRF signal

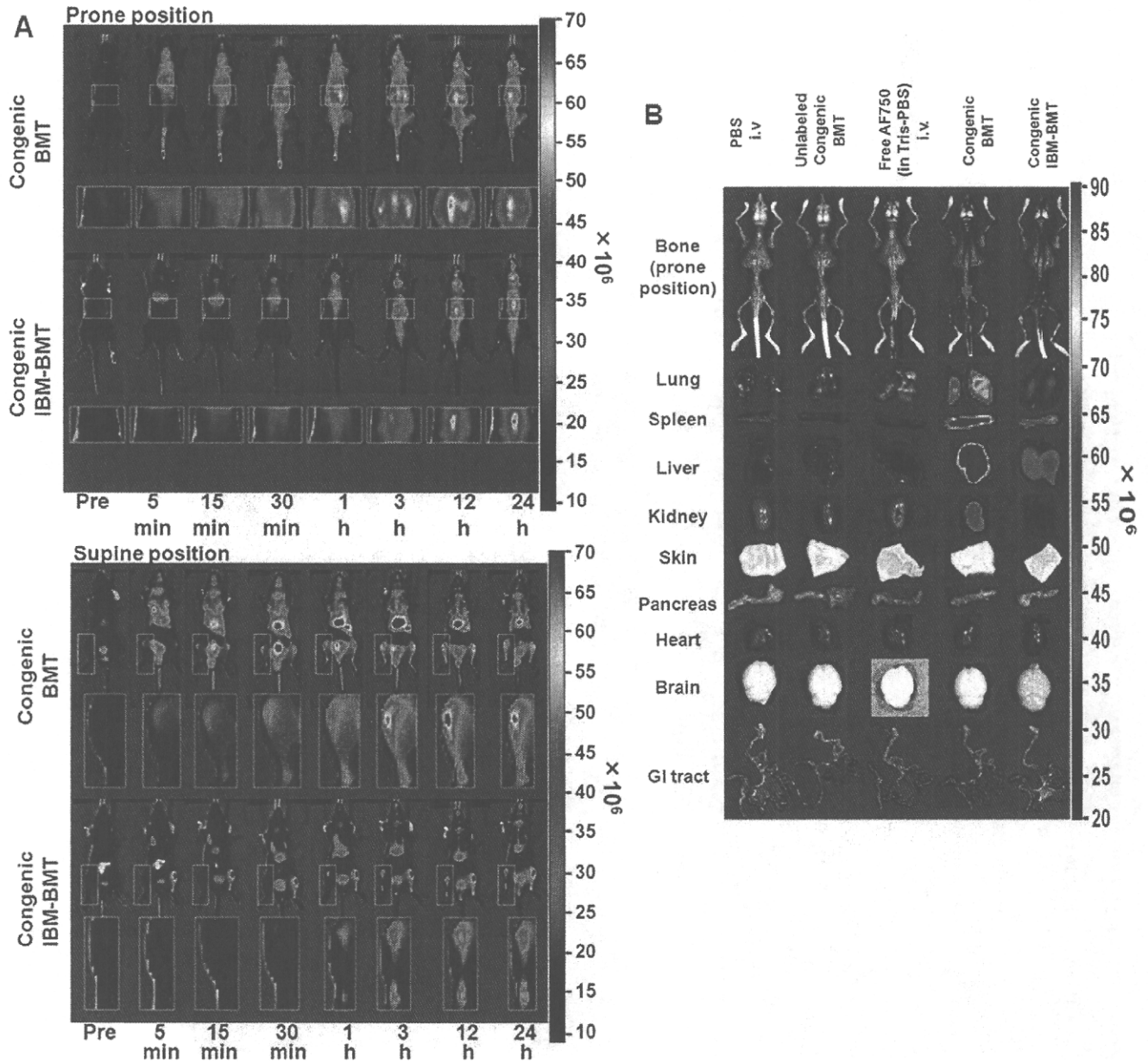

Figure 4. In vivo imaging of transplanted AF750-labeled donor cells in various congenic BMT models. (A) In vivo imaging of congenic BMT models until 24 h after BMT. In the congenic BMT model, the transplanted cells were detected in the tibiae at 5 min after congenic BMT (supine position). In the congenic IBM-BMT model, the migrating cells from the left tibia were detected 1 h after congenic IBM-BMT. The parts of the body with significantly increased signals (indicated by squares) were magnified and are shown below the corresponding whole-body images. (B) Ex vivo imaging of transplanted AF750-labeled donor cells in the BMT models at 24 h after BMT.
doi:10.1371/journal.pone.0011114.g004

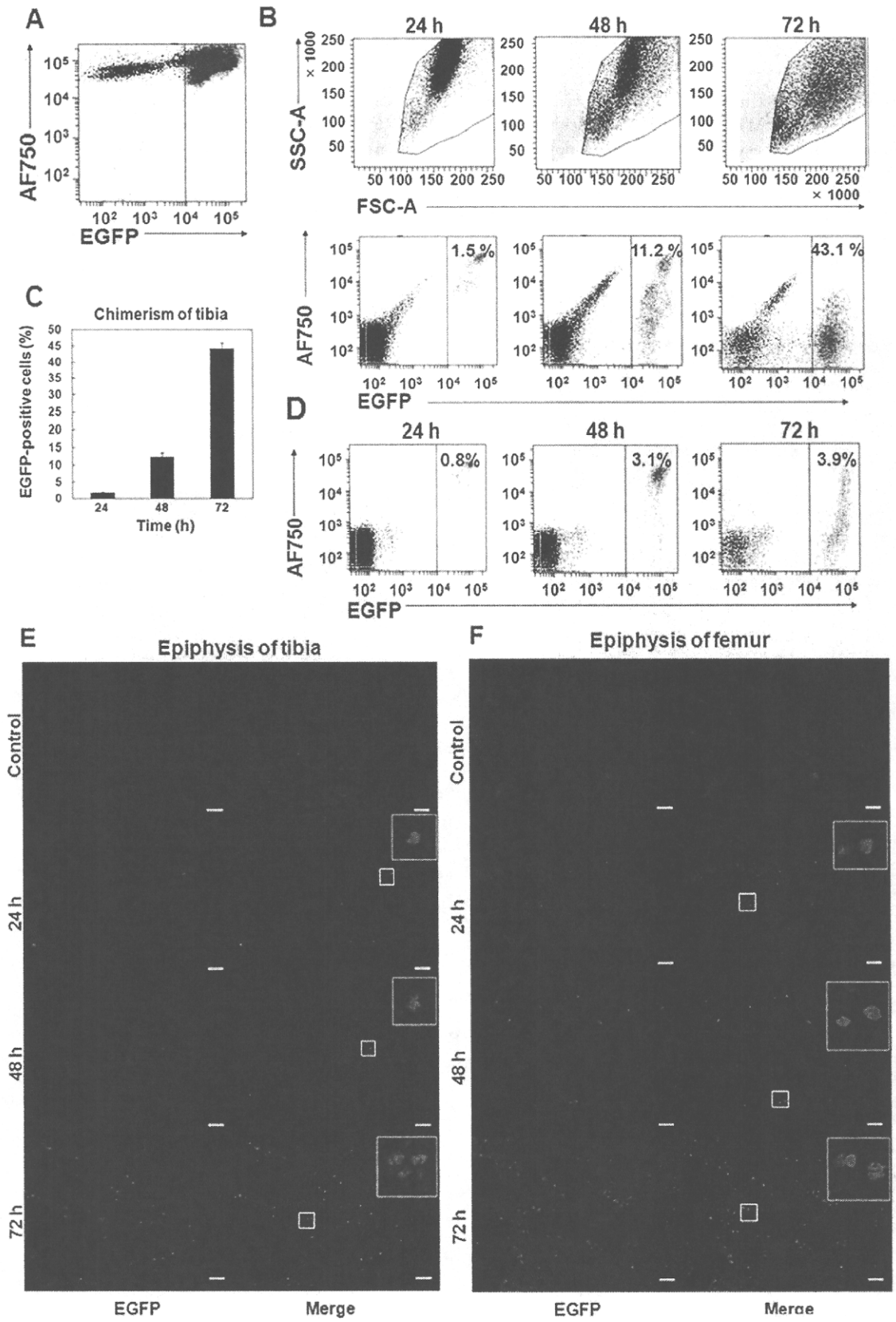

Figure 5. Homing donor cells start cell division at least 24 h after BMT. (A) FACS analysis of AF750-labeled donor ICR/EGFP BM-MNCs was performed immediately after labeling. (B) Chimerism of the transplanted donor AF750/EGFP double-positive cells in the tibiae. Lethally irradiated Balb/c nu/nu recipients (H-2^d) were transplanted with 1×10^7 AF750-labeled ICR/EGFP BM-MNCs. The cells in the tibiae were harvested, and $EGFP^+$ cells were analyzed by FACS at the indicated times after BMT. (C) Mean% ± SEM of $EGFP^+$ cells in the recipient tibiae at the indicated times after BMT

(n = 4). (D) The chimerism of EGFP$^+$ cells in the peripheral blood of the mice in (B) was analyzed by FACS. (E, F) Representative fluorescence images of the tibiae (E) and femora (F). The bones were removed from the mice at the indicated times after BMT. Slices (3-μm thick) of the tibial and femoral epiphyses were observed with an inverted fluorescent microscope. Donor EGFP$^+$ cells rapidly expanded in the tibial and femoral epiphyses between 48 and 72 h after BMT. Untreated Balb/c nu/nu mice were used as controls. Green, EGFP; blue, DAPI. Bar = 100 μm.
doi:10.1371/journal.pone.0011114.g005

detection sensitivity; and (5) our original fasting protocol successfully excluded autofluorescence derived from food particles, the major obstacle in precise imaging of the abdomen.

Balb/c nu/nu mice lack the *whn* gene [17,18], which encodes a forkhead/winged-helix transcription factor confined to expression in the thymic epithelium, epidermis, and hair follicles. As a result of the *whn* gene deficiency, Balb/c nu/nu mice lack the thymus and post-thymic mature T cells [19]. However, this gene is not expressed in HSCs [20], and reduction in the function of antigen-presenting cells such as macrophages and dendritic cells of Balb/c nu/nu mice has not been reported. Therefore, there is little possibility that their genetic defect influences early transplantation events such as homing of HSCs or antigen presentation in GVHD.

Abdominal autofluorescence caused by food disturbs precise evaluation of in vivo imaging. To suppress autofluorescence from food particles in the GI tract, all mice were fasted according to our original fasting protocol prior to in vivo imaging (Supplemental Fig. S1). As a result of fasting, the autofluorescence of the GI tract was dramatically attenuated in vivo and ex vivo (Supplemental Fig. S6). Obvious fasting-related organ damage was not apparent in these mice (Supplemental Fig. S6).

Homing of AF750-labeled donor cells in the tibiae was detected less than 1 h after BMT in the congenic BMT model. Signals from the tibia were noted at 3 h after transplantation and continued to rise until 24 h after transplantation. IBM-BMT is a method of transplanting HSCs and stromal cells directly into niches in the BM cavity [21,22], and the kinetics and homing of the transplanted cells to all the bones of the body after IBM-BMT have not been determined previously. In this study, we elucidated that most of the transplanted cells remained within the injected tibia, while some cells entered the peripheral circulation though the BM sinus of the tibia, and cells trapped in the lung were observed 5 min after IBM-BMT. Moreover, circulating cells started migrating to the backbone and the collateral tibia of the injected site 1 h after IBM-BMT.

FACS analysis using ICR/EGFP as donors revealed that transplanted donor cells started cell division more than 24 h after BMT and that hematopoietic reconstitution in Balb/c nu/nu mice

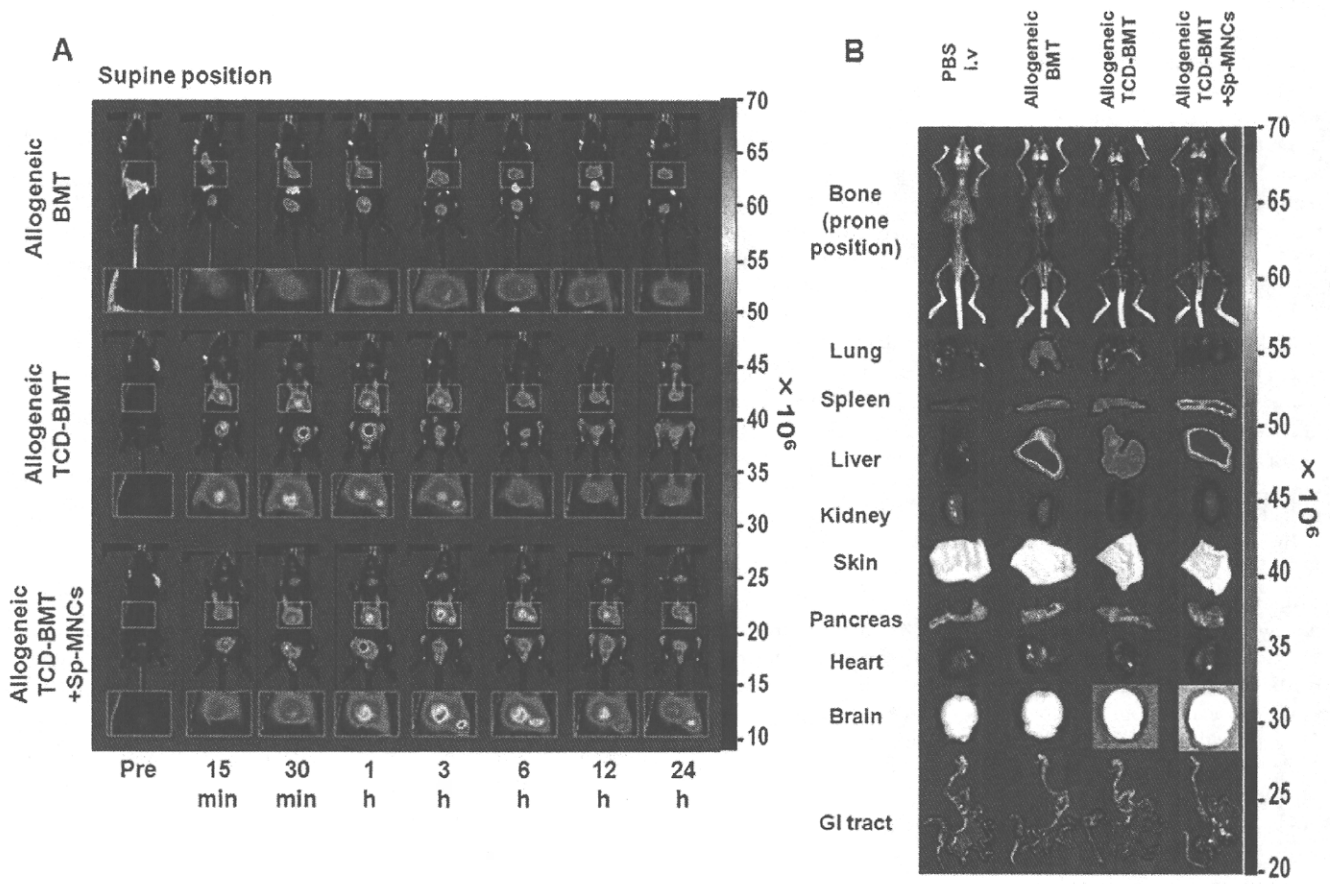

Figure 6. In vivo imaging of transplanted AF750-labeled donor cells in various allogeneic BMT models. (A) In vivo imaging of allogeneic BMT models until 24 h after BMT. Conditioned Balb/c nu/nu recipients (H-2^d) received 1×10^7 AF750-labeled C57BL/6 BM-MNCs (H-2^b) (upper row), 1×10^7 TCD C57BL/6 BM-MNCs (middle row), or 5×10^6 C57BL/6 TCD BM-MNCs plus 5×10^6 C57BL/6 Sp-MNCs (bottom row). Areas indicated by squares are magnified and shown below each image. (B) Ex vivo imaging of transplanted AF750-labeled donor cells in various allogeneic BMT models at 24 h after BMT.
doi:10.1371/journal.pone.0011114.g006

recipients began approximately 72 h after BMT (Fig. 5), indicating that donor cell homing must have had started within 24 h after BMT. Therefore, it is very important to understand both the homing process of HSCs and mechanisms of engraftment failure for accurate assessment of transplanted donor cell distribution during the very initial phase after BMT.

With regard to aGVHD, Peyer's patches (gut-associated secondary lymphoid organs) are the initial sites of aGVHD [23,24], and it has been previously reported that the infiltration of donor cells into Peyer's patches rapidly increased around 3 days after BMT in murine GVHD models [8]. Furthermore, splenectomy and prevention of T-cell entry into all secondary lymphoid organs with αMAdCAM-1 and αCD62L monoclonal antibodies abrogated the onset of gut GVHD [25]. Considering these reports, gut GVHD would begin within 72 h after BMT, and involvement of all secondary lymphoid organs may be necessary to evoke gut GVHD. Our results regarding the allogeneic BMT and GVHD models revealed that the donor cells were barely detected in the intestinal tract within 24 h, and very few instances of direct homing to Peyer's patches were detected in the allogeneic BMT models. On the other hand, a large number of cells were found trapped in the lung, liver, spleen, and superficial lymph nodes within 24 h after BMT (Fig. 6). Considering these observations, it seems that a larger number of cells was present in the reticuloendothelial system than in Peyer's patches until 24 h after BMT and that the secondary infiltration of T cells from secondary lymphoid organs to Peyer's patches is also considered to be very important for induction of gut GVHD.

The mechanisms of hematopoietic cell homing have not been revealed. It is assumed that the homing of hematopoietic cells is caused by molecular interactions of transplanted cells with their niche components [26,27] and that homing processes are varied among hematopoietic cell populations [28]. As for lymphocytes, high endothelial venules in lymph nodes or secondary lymphoid tissues contribute to continuous immune surveillance by supporting lymphocyte recruitment from the blood [29,30]. Our results clearly revealed that in the initial phase after BMT, the cell distributions were varied among BMT models. For example, in GVHD models, a T-cell population dominantly homed to the reticuloendothelial system, whereas TCD donor cells dominantly homed to BM (Fig. 6B). Using TCD BM-MNCs, which contained less lymphocytes and more hematopoietic cells including HSCs, we demonstrated that transplanted cells primarily homed to BM and secondarily homed to lymphoid organs, including the reticuloendothelial system (Fig. 6B).

In this study, we labeled the surface of transplanted cells with NIRF and successfully demonstrated their altered distribution dynamics during the initial phase. There are several transgenic murine models with unique HSCs or BM microenvironments. Our method may be useful to obtain spatiotemporal information of the donor cell homing process in these mice. Together with other optical imaging techniques such as bioluminescence imaging, we believe that this method would provide a means to study the pivotal process of complications associated with BMT, such as engraftment failure and GVHD, and would contribute to improvement of therapeutic outcomes of BMT.

Supporting Information

Figure S1 (A) Our original fasting protocol. (B) Autofluorescence of the feed and stool of Balb/c mice. Autofluorescence of each solution (C) and compositions (D) of solutions. (E) Evaluation of % body weight change of fasting Balb/c mice (OS-1 versus H2O) (n = 5). (F) Survival curve of mice in (E) (n = 5).
Found at: doi:10.1371/journal.pone.0011114.s001 (2.29 MB TIF)

Figure S2 The proportions of sub-G1 fractions of Balb/c nu/nu BM-MNCs was analyzed by FACS at 2 h after labeling (n = 5). DNA content was analyzed as previously described [13]. The population of cells with degraded genomic DNA (sub-G1 fraction) was identified. Values are mean rates ± SEM for the indicated concentrations.
Found at: doi:10.1371/journal.pone.0011114.s002 (1.72 MB TIF)

Figure S3 Viable Balb/c Sp-MNCs were analyzed by a modified MTT assay. Various concentrations of Cy5.5- or AF750-labeled Sp-MNCs (1×105) were seeded in a 96-well plate with phenol red-free RPMI 1640 medium containing CD3/28 beads and mIL2 (n = 5). The cells were then incubated for the indicated times. At the end of the culture period, the viable cell number was analyzed as previously described [12] with slight modifications. The absorbance (450 nm) was measured 3 h after adding the cell-counting reagent. The experiments were done in at least triplicate, and results are presented as the mean relative OD ± SEM.
Found at: doi:10.1371/journal.pone.0011114.s003 (1.73 MB TIF)

Figure S4 The proportions of sub-G1 fractions caused by a single fraction of near-infrared excitation and emission. NIRF-labeled or unlabeled Balb/c nu/nu BM-MNCs were excited for 5 s using the IVIS (Cy5.5: 640 nm, AF750: 710 nm) and the sub-G1 fractions were analyzed by FACS at 2 h after excitation (n = 5).
Found at: doi:10.1371/journal.pone.0011114.s004 (1.77 MB TIF)

Figure S5 FACS analysis for the decrement of mean fluorescence intensity (MFI) by repeated excitations. NIRF-labeled Balb/c nu/nu BM-MNCs were excited for 5 s per excitation using the IVIS (n = 5). The MFIs of NIRF-labeled BM-MNCs were analyzed by FACS at 2 h after repeated excitation for the indicated times.
Found at: doi:10.1371/journal.pone.0011114.s005 (0.89 MB TIF)

Figure S6 (A,B) Autofluorescence in the abdomen was significantly reduced by the original fasting protocol. (C) Histological analyses (H&E staining) of the indicated organs in fasted mice on day 1. Fasting-related organ damage was not apparent in the fasting mice. Bar = 100 μm.
Found at: doi:10.1371/journal.pone.0011114.s006 (2.62 MB TIF)

Figure S7 In vivo imaging of transplanted Cy5.5-labeled donor cells. In vivo imaging of Cy5.5-labeled Balb/c nu/nu BM-MNCs with mice in the supine and prone positions. Signals for the transplanted Cy5.5-labeled cells were seen in the backbone and the tibia. The areas indicated by squares are magnified and are shown below each image.
Found at: doi:10.1371/journal.pone.0011114.s007 (3.57 MB TIF)

Figure S8 In vivo imaging of transplanted AF750-labeled donor cells. Conditioned recipients were injected with indicated solutions.
Found at: doi:10.1371/journal.pone.0011114.s008 (2.23 MB TIF)

Figure S9 Donor EGFP+ cells appeared in the peripheral blood at 72 h with similar fluorescence intensity to that in the BM. Purple, donor cells; Black, recipient cells.
Found at: doi:10.1371/journal.pone.0011114.s009 (1.15 MB TIF)

Acknowledgments

We are grateful to Youshi Fujita for discussions and technical advice; Atsushi Murakami, Yumi Takahashi, and Taeko Tani for their skilled technical assistance; Gen Kondoh, Hitoshi Miyachi, and Satsuki Kitano for supplying the ICR/EGFP mice; and Kenichi Fukazawa for the FACS analyses.

Author Contributions

Conceived and designed the experiments: TU SKK EA. Performed the experiments: TU EA. Analyzed the data: TU SKK EA MM HH SK YA TM MH. Contributed reagents/materials/analysis tools: SKK EA ST MM HH YA TM MH. Wrote the paper: TU SKK.

References

1. Stotler C, Bolwell B, Sobecks R, Dean R, Serafino S, et al. (2010) Are backup BM harvests worthwhile in unrelated donor allogeneic transplants? Bone Marrow Transplant 45: 49–52.
2. Ferrara JL, Levine JE, Reddy P, Holler E (2009) Graft-versus-host disease. Lancet 373: 1550–1561.
3. Papayannopoulou T (2003) Bone marrow homing: the players, the playfield, and their evolving roles. Curr Opin Hematol 10: 214–219.
4. Papayannopoulou T, Craddock C, Nakamoto B, Priestley GV, Wolf NS (1995) The VLA4/VCAM-1 adhesion pathway defines contrasting mechanisms of lodgement of transplanted murine hemopoietic progenitors between bone marrow and spleen. Proc Natl Acad Sci U S A 92: 9647–9651.
5. Srour EF, Jetmore A, Wolber FM, Plett PA, Abonour R, et al. (2001) Homing, cell cycle kinetics and fate of transplanted hematopoietic stem cells. Leukemia 15: 1681–1684.
6. Zhang Y, Shlomchik WD, Joe G, Louboutin JP, Zhu J, et al. (2002) APCs in the liver and spleen recruit activated allogeneic CD8+ T cells to elicit hepatic graft-versus-host disease. J Immunol 169: 7111–7118.
7. Shlomchik WD, Couzens MS, Tang CB, McNiff J, Robert ME, et al. (1999) Prevention of graft versus host disease by inactivation of host antigen-presenting cells. Science 285: 412–415.
8. Panoskaltsis-Mortari A, Price A, Hermanson JR, Taras E, Lees C, et al. (2004) In vivo imaging of graft-versus-host-disease in mice. Blood 103: 3590–3598.
9. Weissleder R, Pittet MJ (2008) Imaging in the era of molecular oncology. Nature 452: 580–589.
10. Steiner D, Gelovani J, Savoldo B, Robinson SN, Decker WK, et al. (2009) Noninvasive bioluminescent imaging demonstrates long-term multilineage engraftment of ex vivo-expanded CD34-selected umbilical cord blood cells. Stem Cells 27: 1932–1940.
11. Okabe M, Ikawa M, Kominami K, Nakanishi T, Nishimune Y (1997) 'Green mice' as a source of ubiquitous green cells. FEBS Lett 407: 313–319.
12. Kizaka-Kondoh S, Itasaka S, Zeng L, Tanaka S, Zhao T, et al. (2009) Selective killing of hypoxia-inducible factor-1-active cells improves survival in a mouse model of invasive and metastatic pancreatic cancer. Clin Cancer Res 15: 3433–3441.
13. Zeng L, Kizaka-Kondoh S, Itasaka S, Xie X, Inoue M, et al. (2007) Hypoxia inducible factor-1 influences sensitivity to paclitaxel of human lung cancer cell lines under normoxic conditions. Cancer Sci 98: 1394–1401.
14. Kushida T, Inaba M, Hisha H, Ichioka N, Esumi T, et al. (2001) Intra-bone marrow injection of allogeneic bone marrow cells: a powerful new strategy for treatment of intractable autoimmune diseases in MRL/lpr mice. Blood 97: 3292–3299.
15. Kolb HJ (2008) Graft-versus-leukemia effects of transplantation and donor lymphocytes. Blood 112: 4371–4383.
16. Kalchenko V, Shivtiel S, Malina V, Lapid K, Haramati S, et al. (2006) Use of lipophilic near-infrared dye in whole-body optical imaging of hematopoietic cell homing. J Biomed Opt 11: 050507.
17. Nehls M, Pfeifer D, Schorpp M, Hedrich H, Boehm T (1994) New member of the winged-helix protein family disrupted in mouse and rat nude mutations. Nature 372: 103–107.
18. Schlake T, Schorpp M, Nehls M, Boehm T (1997) The nude gene encodes a sequence-specific DNA binding protein with homologs in organisms that lack an anticipatory immune system. Proc Natl Acad Sci U S A 94: 3842–3847.
19. Chatterjea-Matthes D, Garcia-Ojeda ME, Dejbakhsh-Jones S, Jerabek L, Manz MG, et al. (2003) Early defect prethymic in bone marrow T cell progenitors in athymic nu/nu mice. J Immunol 171: 1207–1215.
20. Pignata C, Gaetaniello L, Masci AM, Frank J, Christiano A, et al. (2001) Human equivalent of the mouse Nude/SCID phenotype: long-term evaluation of immunologic reconstitution after bone marrow transplantation. Blood 97: 880–885.
21. Li Q, Hisha H, Yasumizu R, Fan TX, Yang GX, et al. (2007) Analyses of very early hemopoietic regeneration after bone marrow transplantation: comparison of intravenous and intrabone marrow routes. Stem Cells 25: 1186–1194.
22. Ikehara S (2003) A novel strategy for allogeneic stem cell transplantation: perfusion method plus intra-bone marrow injection of stem cells. Exp Hematol 31: 1142–1146.
23. Murai M, Yoneyama H, Ezaki T, Suematsu M, Terashima Y, et al. (2003) Peyer's patch is the essential site in initiating murine acute and lethal graft-versus-host reaction. Nat Immunol 4: 154–160.
24. Hill GR, Ferrara JL (2000) The primacy of the gastrointestinal tract as a target organ of acute graft-versus-host disease: rationale for the use of cytokine shields in allogeneic bone marrow transplantation. Blood 95: 2754–2759.
25. Beilhack A, Schulz S, Baker J, Beilhack GF, Nishimura R, et al. (2008) Prevention of acute graft-versus-host disease by blocking T-cell entry to secondary lymphoid organs. Blood 111: 2919–2928.
26. Forsberg EC, Smith-Berdan S (2009) Parsing the niche code: the molecular mechanisms governing hematopoietic stem cell adhesion and differentiation. Haematologica 94: 1477–1481.
27. Kaplan RN, Psaila B, Lyden D (2007) Niche-to-niche migration of bone-marrow-derived cells. Trends Mol Med 13: 72–81.
28. Chavakis E, Urbich C, Dimmeler S (2008) Homing and engraftment of progenitor cells: a prerequisite for cell therapy. J Mol Cell Cardiol 45: 514–522.
29. Vestweber D, Wild MK (2008) A new player in lymphocyte homing. Nat Immunol 9: 347–348.
30. Kanda H, Newton R, Klein R, Morita Y, Gunn MD, et al. (2008) Autotaxin, an ectoenzyme that produces lysophosphatidic acid, promotes the entry of lymphocytes into secondary lymphoid organs. Nat Immunol 9: 415–423.

European Journal of Immunology

Galectin-9 ameliorates acute GVH disease through the induction of T-cell apoptosis

Kazuki Sakai[*1,2], *Eri Kawata*[*1], *Eishi Ashihara*[1], *Yoko Nakagawa*[1], *Akira Yamauchi*[3], *Hisayuki Yao*[1], *Rina Nagao*[1], *Ruriko Tanaka*[1], *Asumi Yokota*[1], *Miki Takeuchi*[1], *Hideyo Hirai*[1], *Shinya Kimura*[4], *Mitsuomi Hirashima*[5], *Norio Yoshimura*[2] *and Taira Maekawa*[1]

[1] Department of Transfusion Medicine and Cell Therapy, Kyoto University Hospital, Kyoto, Japan
[2] Department of Transplantation and Regenerative Surgery, Kyoto Prefectural University of Medicine, Japan
[3] Department of Cell Regulation, Faculty of Medicine, Kagawa University, Japan
[4] Division of Hematology, Respiratory Medicine, and Oncology, Department of Internal Medicine, Faculty of Medicine, Saga University, Japan
[5] Department of Immunology and Immunopathology, Faculty of Medicine, Kagawa University, Japan

Galectins comprise a family of animal lectins that differ in their affinity for β-galactosides. Galectin-9 (Gal-9) is a tandem-repeat-type galectin that was recently shown to function as a ligand for T-cell immunoglobin domain and mucin domain-3 (Tim-3) expressed on terminally differentiated $CD4^+$ Th1 cells. Gal-9 modulates immune reactions, including the induction of apoptosis in Th1 cells. In this study, we investigated the effects of Gal-9 in murine models of acute GVH disease (aGVHD). First, we demonstrated that recombinant human Gal-9 inhibit MLR in a dose-dependent manner, involving both Ca^{2+} influx and apoptosis in T cells. Next, we revealed that recombinant human Gal-9 significantly inhibit the progression of aGVHD in murine BM transplantation models. In conclusion, Gal-9 ameliorates aGVHD, possibly by inducing T-cell apoptosis, suggesting that gal-9 may be an attractive candidate for the treatment of aGVHD.

Key words: Apoptosis · Galectin-9 · GVH disease

Supporting Information available online

Introduction

Galectins comprise a family of animal lectins that preferentially bind to β-galactosides through a carbohydrate recognition domain. The 15 members of the galectin family are divided into three groups based on structural similarities [1, 2]. Among the members of the galectin family, Galectin-9 (Gal-9) belongs to the group of bivalent tandem repeat galectins and has two homologous carbohydrate recognition domains connected by a linker peptide [3]. Gal-9 was initially characterized as an eosinophil-specific chemoattractant [4] and, subsequently, Gal-9 was found to possess a variety of biological functions, including roles in cell differentiation, aggregation, adhesion, the induction of cell death, and the inhibition of cancer metastasis [5–8].

Gal-9 is a ligand for T-cell immunoglobin domain and mucin domain-3 (Tim-3) expressed on terminally differentiated $CD4^+$

Correspondence: Dr. Eishi Ashihara
e-mail: ash0325@kuhp.kyoto-u.ac.jp, ash@koto.kpu-m.ac.jp

*These authors contributed equally to this work.

Th1 cells. Gal-9 induces the loss of IFN-γ-producing Th1 cells, thereby negatively regulating Th1 autoimmunity in EAE [9]. The suppression of immune reactions by Gal-9 has also been shown in other Th1-mediated disease models [10, 11]. In the current study, we investigated the immunosuppressive effects of Gal-9 using a murine BM transplantation (BMT) model. We demonstrated that recombinant human (rh) Gal-9 suppresses the induction of acute GVH disease (aGVHD) by inducing T-cell apoptosis.

Results

Gal-9 inhibits MLR through the induction of T-cell apoptosis

We first examined whether Gal-9 inhibited MLR. Splenic mononuclear cells were isolated from C57BL/6 and B6D2F1 female mice, and then 5×10^6 C57BL/6 splenocytes (responders) were cocultured with 1×10^5 irradiated B6D2F1 splenocytes (stimulators) in the presence of various concentrations of Gal-9. Gal-9 suppressed the MLR in a dose-dependent manner (Fig. 1A). To investigate whether Gal-9 induced T-cell apoptosis, enriched T cells isolated from the spleens of C57BL/6 mice were cultured in anti-CD3 Ab-coated plates in the presence of serial dilutions of rhGal-9 for 72 h. Similar to a previous report [5], Gal-9 induced apoptosis in a dose-dependent manner (Fig. 1A). We also investigated the effect of Gal-9 on the proliferation of T cells stimulated with anti-CD3 and anti-CD28 Ab. Gal-9 inhibited T-cell proliferation by more than 90% at a dose of 0.03 μM (Fig. 1B). Since the galectin family members bind to sugar chains containing β-galactoside such as lactose [6], we investigated whether lactose inhibited the effects of Gal-9. The addition of 30 mM lactose almost completely abrogated Gal-9-induced cell proliferation (Fig. 1C). To investigate whether Ca^{2+} influx could be involved in the effects of Gal-9 binding to β-galactoside, we performed fluo-4/AM assays of Ca^{2+} influx in response to 1.0 μM Gal-9 treatment. An influx of Ca^{2+} was observed in splenic T cells 10–20 ms after Gal-9 treatment, and lactose reduced the influx of Ca^{2+} induced by Gal-9 (Fig. 1D). Taken together, these results suggest that Gal-9

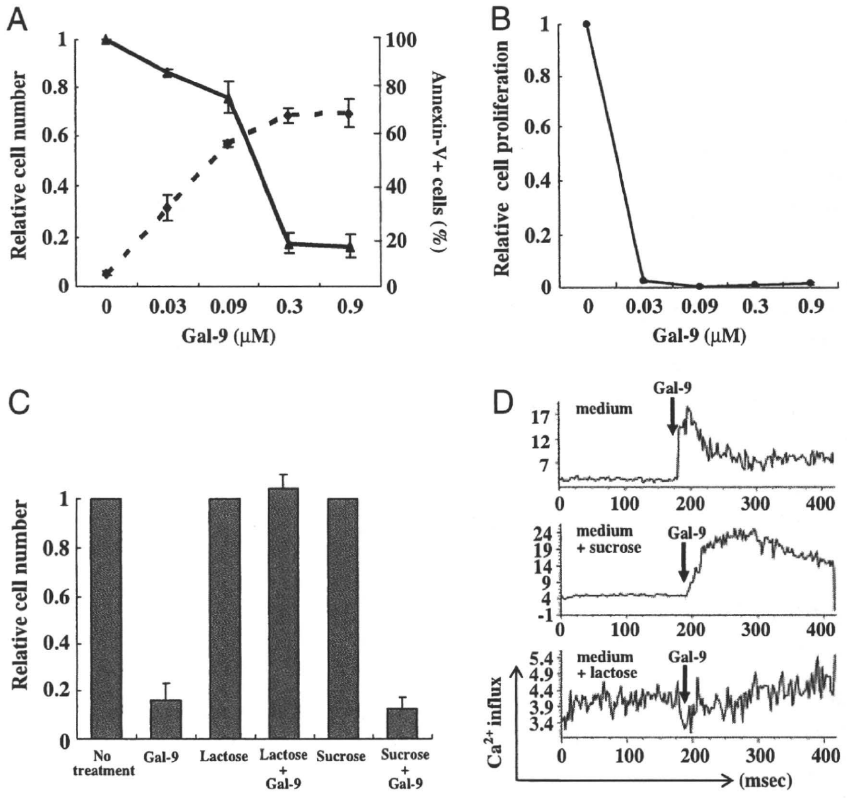

Figure 1. Gal-9 inhibits MLR through the induction of T-cell-apoptosis by Ca^{2+} influx in response to β-galactoside binding. (A) Responder C57BL/6 and irradiated (30 Gy) stimulator B6D2F1 splenocytes were cocultured with rhGal-9 for 10 days. MLR was evaluated by the modified MTT assay (relative cell number, solid line). Enriched T cells obtained from the spleens of C57BL/6 mice were cultured with plate-bound anti-CD3 Ab and rhGal-9 for 72 h. Apoptosis was evaluated by Annexin-V staining (dotted line). (B) Enriched T cells were cultured with plate-bound anti-CD3 Ab, soluble anti-CD28 Ab (5 μg/mL), recombinant mouse IL-2 (20 ng/mL), and rhGal-9. Cell proliferation was assessed by a modified MTT assay after 72 h incubation. (C) A modified MTT assay using splenic T cells after 72 h incubation in the presence of lactose or sucrose (30 mM) and/or rhGal-9 was performed. The data shows relative cell number compared with that without stimulation of lactose, sucrose, or rhGal-9. (D) Splenic T cells in RPMI1640 medium containing 10% FCS with or without sucrose or lactose were loaded with fluo-4/AM (5 μM) and intracellular Ca^{2+} influx after the administration of Gal-9 (1.0 μM; arrow) was measured by FACS Canto II. Data are (A–C) mean ± SD of three experiments (in (B) the SD are smaller than the symbol size and are not visible) and (D) are representative of three independent experiments.

induces T-cell apoptosis, presumably through the modulation of Ca^{2+} influx induced by Gal-9 binding to β-galactoside, resulting in the suppression of MLR.

Gal-9 treatment ameliorates aGVHD

Allogeneic T-cell-depleted BM (TCD-BM) cells and splenocytes from C57BL/6 mice were transplanted into irradiated B6D2F1 mice, and aGVHD was allowed to develop, at which point rhGal-9 was administered i.p. at a dose of 3 or 30 μg/mouse for 14 consecutive days. aGVHD was evaluated by clinical score [12]. The administration of Gal-9 at a dose of 30 μg/mouse significantly ameliorated aGVHD as compared with vehicle-treated mice or mice treated at the dose of 3 μg/mouse (Fig. 2A). However, Gal-9 did not prolong the survival of Gal-9-treated mice as compared with the untreated mice (data not shown). We evaluated pathological scores for

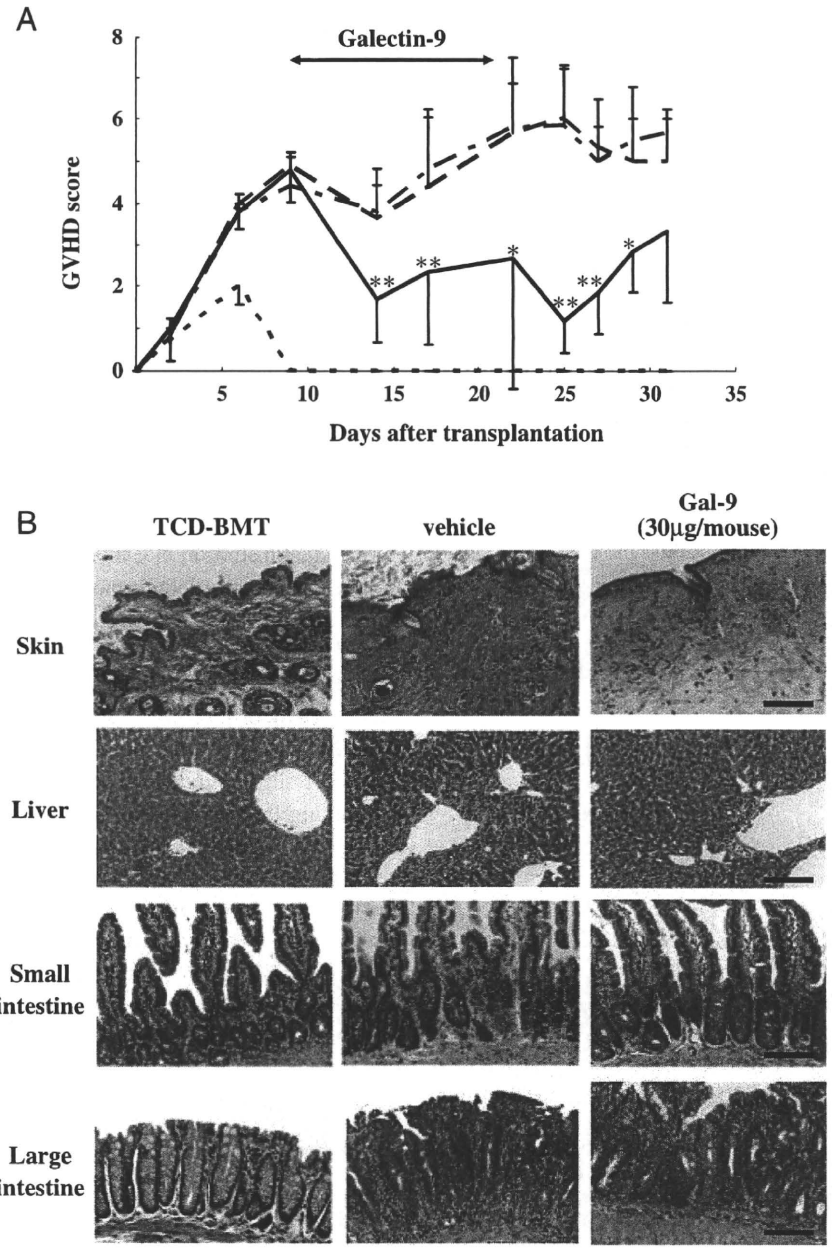

Figure 2. rhGal-9 ameliorates aGVHD in BMT model using mononuclear splenocytes. (A) B5D2F1 mice ($n = 10$ *per* group) were transplanted either with C57BL/6 TCD-MB cells alone and left untreated (dotted line) or with TCD-BM cells and C57Bl/6 mononuclear splenocytes, and once aGVHD had developed, were treated for 14 days with rhGal-9 (3 μg/mouse, dashed line; 30 μg/mouse, solid line) or vehicle alone (dashed, dotted line). Clinical scores were evaluated once or twice a wk. *$p<0.05$; **$p<0.01$ *versus* vehicle control mice (Student's *t*-test). Data are representative of two independent experiments. (B) Histopathological analysis of tissue from recipient mice in the experiments described in (A) stained with hematoxylin and eosin. Tissues were harvested on the day following the administration of rhGal-9 for 14 days. Original magnification, × 200. Each scale bar indicates 100 μm.

Table 1. Histological scores of aGVHD after Gal-9 treatment[a)]

	TCD-BMT	Allo-BMT vehicle	Allo-BMT Gal-9 3 μg	Allo-BMT Gal-9 30 μg
Small intestine	3.5±1.0‡	12.3±3.5	7.8±2.8*	8.2±3.0*
Large intestine	2.2±1.5‡	19.4±2.2	16.7±3.9*	14.8±3.2*
Liver	0.75±0.46‡	9.6±2.0	4.8±1.6†	5.5±2.3†
Total score	6.4±1.6‡	41.3±3.6	29.3±6.3†	28.6±4.6†

[a)] Scores (0–4) for each parameter were assessed on coded slides as described in the *Materials and methods*. Small intestine: villous blunting, crypt regeneration, loss of enterocyte brush border, luminal sloughing of cellular debris, crypt cell apoptosis, outright crypt destruction, and lamina propria lymphocyte infiltrate. Large intestine: crypt regeneration, crypt cell apoptosis, surface colonocyte, colonocyte vacuolization, surface colonocyte attenuation, outright crypt destruction, and lamina propria lymphocyte infiltrate. Liver: portal tract expansion by an inflammatory cell infiltrate, lymphocytic infiltrate of bile ducts, bile duct epithelial cell apoptosis, bile duct epithelial cell sloughing, vascular endothelialitis, parenchymal apoptosis, parenchymal microabscesses, parenchymal mitotic figures, hepatocellular cholestasis, and hepatocellular steatosis. Total GVHD score represents the mean±SD of the sum of scores for small intestine, large intestine, and liver for each animals in indicated group (n = 6–9). *p<0.05 *versus* Allo-BMT treated with vehicle; †p<0.01 *versus* Allo-BMT treated with vehicle; ‡p<0.005 *versus* Allo-BMT treated with vehicle.

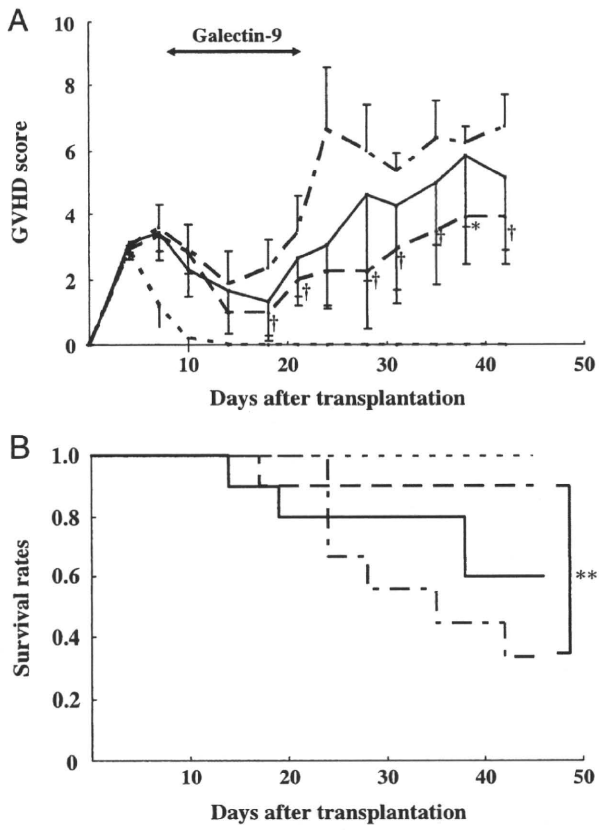

Figure 3. rhGal-9 ameliorates aGVHD in a BMT model using splenic $CD4^+$ T cells. (A) Mice were treated and evaluated as described in Fig. 2A but substituting splenic $CD4^+$ T cells for mononuclear splenocytes. *p<0.01; †p<0.005 *versus* vehicle control mice (Student's t-test). Data are representative of two independent experiments. (B) Survival curves of the $CD4^+$ T-cell-transplanted mice described in (A). **p<0.05 *versus* vehicle control mice (Log-rank test).

the small and large intestines and livers of transplanted mice using a semi-quantitative scoring system described previously [13]. Treatment with Gal-9 at a dose of 3 or 30 μg/mouse significantly decreased damage to these organs in recipient mice (Fig. 2B, Table 1).

We next investigated whether rhGal-9 ameliorated aGVHD induced by the infusion of splenic $CD4^+$ T cells. T-cell-depleted BM (TCD-BM) cells and $CD4^+$ T cells from C57BL/6 mice were transplanted into irradiated B6D2F1 mice. In this system, administration of rhGal-9 significantly ameliorated aGVHD (Fig. 3A). Moreover, administration of Gal-9 at a dose of 3 μg/mouse also prolonged survival as compared with untreated mice (p<0.05, Fig. 3B).

We next investigated the effects of rhGal-9 treatment on $CD4^+$ T-cell subsets. Peripheral blood leukocytes from recipient mice were collected for flow cytometric analysis on the day after a 14-day administration of Gal-9. To analyze the effect of Gal-9 on donor lymphocytes, splenic mononuclear cells from GFP Tg mice were used for the induction of aGVHD. For flow cytometry, the gating parameter was first set to isolate the lymphocyte population of peripheral blood leukocytes, and then set for GFP^+ cells. The frequency of $CD4^+$/Tim-3^+ cells was slightly decreased, whereas, the frequency of $CD4^+$/$CD25^+$ and $CD25^+$/Foxp3^+ Treg was slightly increased, by the Gal-9 treatment (Fig. 4A, Supporting Information Fig. 1); however, the changes were not statistically significant. We also investigated the effects of Gal-9 on cytokine production. Peripheral blood from recipient mice treated with vehicle or rhGal-9 (30 μg/mouse) was collected on the day after a 14-day administration of Gal-9. The production of TNF-α and IL-17 was suppressed by Gal-9 treatment (p = 0.09 and p = 0.03, respectively). Although the production of IFN-γ was decreased, there was no significant difference between the vehicle and Gal-9 treatment groups. IL-2 and IL-10 were unaffected by Gal-9 (Fig. 4B).

Discussion

aGVHD is a serious complication of allogeneic BMT, initiated by damage to the gastrointestinal tract, especially the intestinal mucosa. In the gastrointestinal tract, the bacterial product lipopolysaccharide translocates from the intestinal lumen to the blood circulation and stimulates the secretion of IL-1α and TNF-α from host Mϕ, resulting in the activation of host APC and the

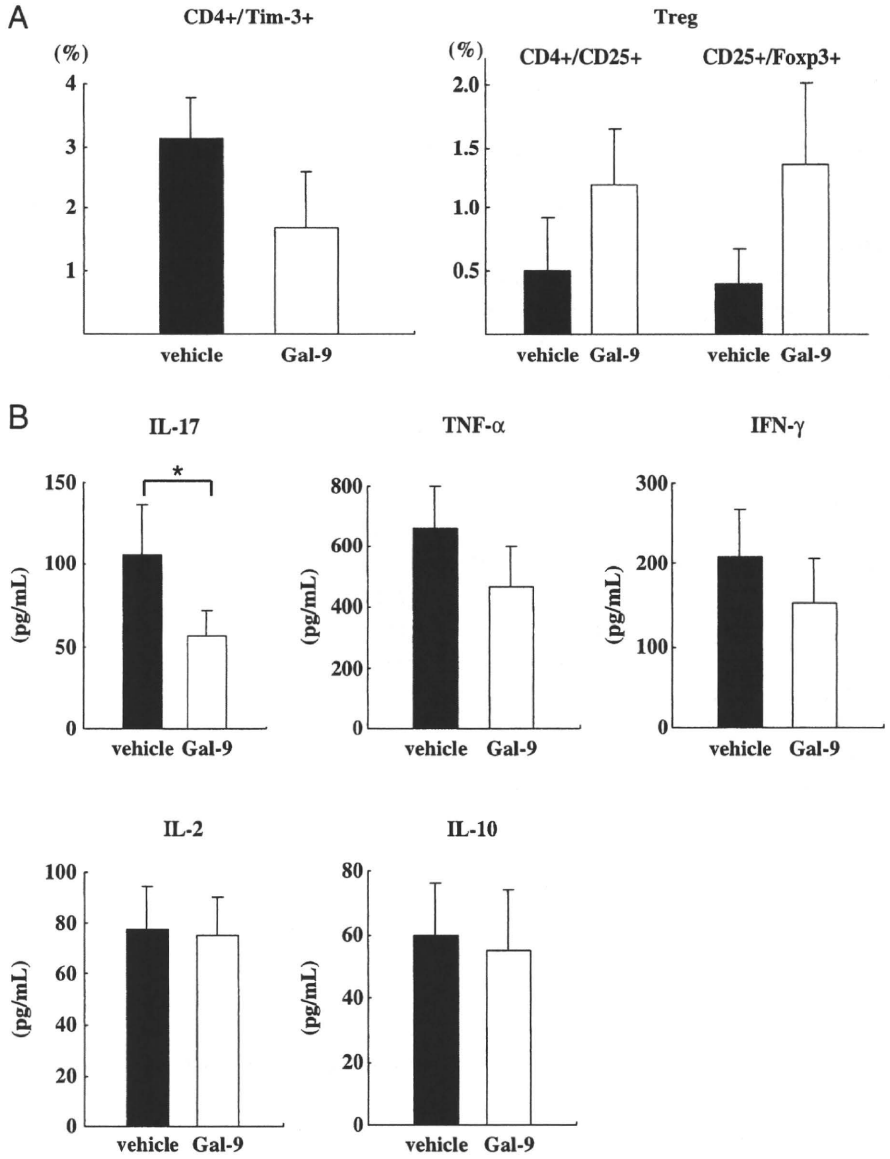

Figure 4. Effects of Gal-9 treatment on $CD4^+$ T-cell subsets and cytokine production. (A) TCD-BM cells obtained from C57Bl/6 mice and splenic mononuclear cells obtained from GFP Tg mice were transplanted into B6D2F1 mice. After induction of aGVHD, vehicle control or 30 μg of rhGal-9 was administered for 14 days. Peripheral blood cells were harvested on the day following the 14 day's administration and T-cell subsets were analyzed by FACS. Data are mean+SD ($n = 3$ *per* group) of two independent experiments giving consistent results. (B) Peripheral blood was collected from the recipient mice on the day following the administration of rhGal-9 or vehicle control for 14 days and the serum was separated to assess cytokine levels ($n = 4$–5 *per* group). Cytokine assays were performed using a Bio-Plex™ Pro Mouse Cytokine Assay. Data are mean+SD of three independent experiments. *$p<0.05$ *versus* vehicle control mice (Student's *t*-test).

differentiation of donor T cells to Th1 cells. Alloreactive Th1 cells release IFN-γ and IL-2, which promote the differentiation of cytotoxic T cells and inflammatory cytokine storms. The consequence of these immune responses is the development of aGVHD in the target organs [14].

In the current study, Gal-9 was found to suppress MLR in a dose-dependent manner, and it was revealed by FACS analysis that Gal-9 treatment increased the number of Annexin-V^+ T cells *in vitro*. Moreover, Gal-9 inhibited the proliferation of $CD3^+$ T cells stimulated with anti-CD3 and anti-CD28 Abs at a dose of only 0.03 μM. Differences in inhibitory doses of Gal-9 between MLR (Fig. 1A) and the T-cell proliferation stimulated with anti-CD3 and anti-CD28 Ab (Fig. 1B) could be due to the activation of DC by Gal-9 in the MLR [15, 16]. We have previously demonstrated that apoptosis is induced in both activated $CD4^+$ and $CD8^+$ T cells, although particularly in the $CD4^+$ T cells through the Ca^{2+}–calpain–caspase-1 pathway [5]. We confirmed here that Gal-9 induces an influx of Ca^{2+} into splenic T cells and that the influx was inhibited by co-treatment with lactose as previously reported [5]. Our findings indicate that Gal-9 induces apoptosis in splenic T cells through Ca^{2+} influx induced by β-galactoside binding, resulting in the suppression of MLR.

We investigated the immunosuppressive effects of Gal-9 in a murine model of aGVHD. rhGal-9 was administered when mice

exhibited symptoms of aGVHD. To clarify the effect of Gal-9 on aGVHD, we administered Gal-9 starting on the day when the influence of radiation was no longer apparent and aGVHD became pronounced. rhGal-9 amerliorated aGVHD clinical scores, and histological analysis revealed that Gal-9 significantly suppressed damage in target organs. However, survival rates in the Gal9-treated mice were not significantly affected as compared with untreated mice (data not shown). One reason for this lack of effect on survival may be the short duration of rhGal-9 treatment. The form of Gal-9 used in the current study is an rh form of the protein and, when rhGal-9 was administered to mice for 2 wk, neutralizing Ab against rhGal-9 were produced and the activity of Gal-9 was diminished (unpublished observations from Dr. Niki in GalPharma). In our preliminary experiments, aGVHD was not controlled any further upon longer treatment (data not shown); thus, we terminated rhGal-9 treatment after 2 wk. Nevertheless, the clinical scores and histological damages induced by aGVHD were improved, even with this short Gal-9 treatment.

The effects of rhGal-9 on aGVHD were also investigated in a $CD4^+$ T-cell-transplanted model. rhGal-9 at a dose of 3 μg/mouse ameliorated aGVHD and prolonged survival as compared with untreated mice. Together with the results of the mononuclear splenocyte-transplanted model, these results indicated that Gal-9 is an effective agent for the treatment of aGVHD. Interestingly, Gal-9 at the higher dose (30 μg/mouse) did not ameliorate aGVHD in the $CD4^+$ T-cell-transplanted model. The reason for this is not clear; however, $CD8^+$ T cells were not transfused into recipient mice in this murine model and aGVHD might not be as aggressive in this model as in the whole splenocyte-transplanted model. We speculate that Gal-9 at the lower dose suppresses aGVHD progression through ;Tim-3, which is expressed on $CD4^+$ T cells. The higher dose of Gal-9, on the other hand, might also activate APC cells [15, 16]. Thus, the inhibitory effects on aGVHD due to the induction of apoptosis may be negated by the APC activation at a higher dose. However, further investigation is necessary to clarify the mechanism by which Gal-9 acts in the context of activated immune functions.

Using splenic mononuclear cells from GFP Tg mice for the induction of aGVHD, we analyzed the effects of Gal-9 treatment on subsets of donor-derived $CD4^+$ T cells. Gal-9 treatment decreased numbers of $CD4^+$/Tim-3^+ T cells and given that Tim-3 is a receptor for Gal-9 [9], these results suggest that Gal-9 may directly induce apoptosis in $CD4^+$/Tim-3^+ T cells. $CD4^+$/$CD25^+$ or $CD25^+$/$Foxp3^+$ Treg numbers in the circulation were, on the other hand, increased by Gal-9 treatment. Treg are involved in the pathogenesis of autoimmune diseases, as well as in immunotolerance in GVHD [17–19]. We have previously shown that there is a significant decrease in $CD4^+$/$Foxp3^+$ splenic cells in Gal-9-deficient mice as compared with WT mice, and that Gal-9 induces the differentiation of $CD4^+$/$CD62L^+$ naive T cells into $Foxp3^+$/$CD4^+$/$CD25^+$ Treg cells [10]. More interestingly in our current study, although $CD4^+$/Tim-3^+ T-cell numbers were decreased by Gal-9 treatment, Treg numbers were increased. These results suggest that Treg precursors do not express Tim-3 and that Gal-9 induces the proliferation of Treg cells through receptors other than Tim-3. Additional studies are warranted to clarify the precise mechanisms of induction of Treg cell expansion by Gal-9.

Analysis of cytokine levels revealed that Gal-9 suppressed the production of IL-17, as well as TNF-α and IFN-γ, in recipient mice. Th17 cells, which are IL-17-producing $CD4^+$ T cells [20], play a crucial role in orchestrating the immune reactions that participate in autoimmune diseases [21, 22]. Recent reports indicate that IL-17-producing Th17 cells augment aGVHD [23–25]. Given that Tim-3 is expressed in Th17 cells [10, 26, 27], the current findings suggest that Gal-9 induces apoptosis in Th17 and Th1 cells, resulting in decreased production of IL-17- and Th1-related cytokines such as TNF-α and IFN-γ. Furthermore, it has been reported that Th17 and Treg cells are reciprocally induced [28]. We speculate that Gal-9 treatment suppresses Th17 differentiation, redirecting the process to Treg differentiation. During aGVHD, the IFN-γ levels in Gal-9-treated mice were decreased, although not significantly, whereas the level of IL-17 was significantly suppressed. Since $CD4^+$ T cells can reciprocally differentiate into Th1 and Th17 cells [23], we speculate that the $CD4^+$ T cells that survived might have differentiated into IFN-γ-producing Th1 cells, resulting in only a slight suppression of IFN-γ.

In conclusion, Gal-9 was found to ameliorate aGVHD in a murine model of BMT through the induction of T-cell apoptosis. The results of the current study suggest that Gal-9 may be useful for the treatment of aGVHD and, in light of previously reported data from other allogeneic transplantation models [10, 11, 29], our results suggest that Gal-9 is a promising biological agent for the suppression of immune reactions.

Materials and methods

Mice

Six- to ten-wk-old C57BL/6 mice ($H\text{-}2^b$) and B6D2F1 female mice ($H\text{-}2^{b/d}$) were purchased from Oriental Bio Service (Kyoto, Japan) and SLC Japan (Osaka, Japan), respectively. GFP Tg mice [30, 31] were kindly provided by Dr. Miyazaki (Osaka University, Japan). Mice were maintained on a 12:12 hour light–dark cycle in a specific pathogen-free animal facility at the Kyoto University. Approval for the animal protocols was obtained from the Committee on Animal Research of the Kyoto University Faculty of Medicine.

Isolation of T cells

T-cell populations of interest were obtained from mice using a magnetic cell sorting separation system (Miltenyi, Gladbach, Germany), according to the manufacturer's instructions. A mouse Pan T Isolation Kit (Miltenyi) was used for the isolation of $CD3^+$ T cells. For the isolation of $CD90.2^+$ and $DC4^+$ T cells, an

anti-CD90.2 Ab and an anti-CD4 Ab (Miltenyi) were used, respectively. Isolated cells were stained with an anti-CD3ε Ab (BD Bioscience, Tokyo, Japan) or an anti-CD4 Ab, and the purity of the isolated or depleted cell populations were analyzed by FACS Canto II using Diva software (BD Bioscience).

MLR

Splenocytes were isolated from spleens of C57BL/6 and B6D2F1 mice after cervical dislocation. Spleens were crushed through a sterile mesh and then were filtered through a 70-μm Cell Strainer (BD Bioscience). Single-cell suspensions were prepared in RPMI1640 (Gibco, Tokyo, Japan) containing 10% heat-inactivated FCS (Invitrogen, Tokyo, Japan), 2 mM L-glutamine (Gibco), and 1% penicillin-streptomycin (Gibco), and then mononuclear splenocytes were obtained by Ficoll-Hypaque density centrifugation (Lympholyte-M; Cedarlane, Ontario, Canada). Responder C57BL/6 splenocytes (5×10^6 cells/100 μL *per* well) and irradiated (30 Gy) stimulator B6D2F1 splenocytes (1×10^5 cells/100 μL *per* well) were cocultured in a flat-bottom 96-well plate (BD Bioscience) in the presence of serial dilutions of rhGal-9 for 10 days. MLR was evaluated by a modified MTT assay [32, 33] using a Cell-counting kit-8 (Dojindo Laboratory, Kumamoto, Japan). Data represent the means of four samples for each concentration of Gal-9.

The effect of Gal-9 on T-cell proliferation, stimulated by anti-CD3 and anti-CD28 Ab was evaluated in cultures of enriched splenic T cells from C57BL/6 mice. The purity of the isolated $CD3^+$ T-cell population was more than 95%. T cells were cultured (2.5×10^5/well) in 96-well anti-CD3 Ab-coated plates (BD Bioscience) with soluble anti-CD28 Ab (5 μg/mL; BD Bioscience) and recombinant mouse IL-2 (20 ng/mL; Wako, Osaka, Japan) with or without serial dilutions of rhGal-9. After 72 h, cell proliferation was assessed using a modified MTT assay. Data represent the means of four samples for each concentration of Gal-9.

Analysis of apoptosis

Enriched $CD90.2^+$ T cells were cultured in anti-CD3 Ab-coated plates in the presence or absence of Gal-9 for 72 h. The purity of the enriched cell population was ≥95%, and CD3 expression was confirmed. Apoptosis was determined using an Annexin V-FITC Apoptosis Detection Kit I (BD Bioscience), according to the manufacturer's instructions. Cells were analyzed by FACS Canto II using Diva software. To assess the requirement for β-galactoside binding in Gal-9-induced apoptosis, we performed a modified MTT assay using splenic T cells in the presence of 30 mM lactose or sucrose (Wako).

Ca^{2+} influx

Splenic T cells in RPMI1640 medium containing 10% FCS were loaded with fluo-4/AM (5 μM) (Invitrogen) at 37°C for 30 min. Cells were washed and resuspended in medium, and then intracellular Ca^{2+} influx induced in response to rhGal-9 (1.0 μM) was measured using FACS Canto II. Data were analyzed using FlowJo software (Tree Star, Ashland, OR) We also evaluated the requirement of β-galactoside binding in Ca^{2+} influx by culturing cells in the presence of lactose or sucrose (30 mM).

BMT

WT C57BL/6 mice were sacrificed by cervical dislocation, and femurs and tibiae were removed. BM cells were collected by flushing bones with RPIM1640 containing 10% FCS using a 21-gauge needle, and then the cells were filtered and washed twice by centrifugation at 1500 rpm for 5 min. After the BM cells were suspended in buffer (1 × PBS containing 5 mM EDTA and 0.5% BSA), T-cell-depletion was performed using an anti-CD90.2 Ab. Residual $CD90.2^+$ cells were routinely less than 0.5% of purified BM cells. TCD-BM cells were resuspended in 1 × PBS prior to injection. Mononuclear splenocytes from WT C57BL/6 mice were used as the source of allogeneic T cells. Recipient B6D2F1 mice received a myeloablative dose (9 Gy) of total body irradiation from an X-ray irradiator. Six to eight hours later, each recipient mouse was injected i.v. with 4×10^6 TCD-BM cells alone or with 5×10^6 mononuclear splenocytes. Where indicated, the ability of rhGal-9 to ameliorate aGVHD induced by splenic $CD4^+$ T cells was evaluated. The purity of the enriched $CD4^+$ T-cell population was more than 95%. Recipient B6D2F1 mice received a myeloablative dose (9 Gy) of total body irradiation, and then each recipient mouse was injected i.v. with 4×10^6 TCD-BM cells with or without 2×10^6 $CD4^+$ splenocytes.

aGVHD and Gal-9 treatment

aGVHD clinical scores were evaluated once or twice a wk [12]. After aGVHD developed, recipient mice were treated with rhGal-9 (3 or 30 μg/mouse) or vehicle by i.p. injection for 14 consecutive days. Mice that exhibited aGVHD score of greater than 7 were sacrificed and added to the Kaplan–Meier statistics the same day, as previously reported [34]. Histopathological evaluation of aGVHD was performed as follows. Tissues (liver, skin, and small and large intestines) from the recipient mice were placed in 10% formalin, embedded in paraffin, sectioned, and then stained with hematoxylin and eosin. Slides were coded without reference to prior treatment and examined in a blinded fashion by one individual (E.A.). A semi-quantitative scoring system was used as previously described [13]. Seven parameters were scored for the small intestine (villous blunting, crypt regeneration, loss of enterocyte brush border, luminal sloughing of cellular debris, crypt cell apoptosis, outright crypt destruction, and lamina propria lymphocyte infiltrate) and large intestine (crypt regeneration, crypt cell apoptosis, surface colonocyte, colonocyte vacuolization, surface colonocyte attenuation, outright crypt

destruction, and lamina propria lymphocyte infiltrate); and ten parameters were scored for the liver (portal tract expansion by an inflammatory cell infiltrate, lymphocytic infiltrate of bile ducts, bile duct epithelial cell apoptosis, bile duct epithelial cell sloughing, vascular endothelialitis, parenchymal apoptosis, parenchymal microabscesses, parenchymal mitotic figures, hepatocellular cholestasis, and hepatocellular steatosis). The scoring system was as follows: 0 = normal; 0.5 = focal and rare; 1 = focal and mild; 2 = diffuse and mild; 3 = diffuse and moderate; and 4 = diffuse and severe. Scores were added to provide a total score for each organ. The maximum score for the small intestine and large intestine was 28, and for the liver, 40.

Phenotypic analysis of $CD4^+$ T-cell subsets

Peripheral blood leukocytes from recipient mice were collected for flow cytometric analysis of $CD4^+$ T-cell subsets on the day following the administration of Gal-9 for 14 days. To analyze donor lymphocytes, the splenic mononuclear cells obtained from GFP Tg mice were used for the induction of aGVHD. The gating parameters were first set to isolate the lymphocyte population of peripheral blood leukocytes, and then set to isolate GFP^+ cells. T-cell subsets were analyzed using the following Ab: anti-mouse CD4-PerCP-Cy5.5 (eBioscience, San Diego, CA), anti-mouse Tim-3-PE (eBioscience), anti-CD25-PE, and anti-Foxp3-allophycocyanin (eBioscience). Cells were analyzed by FACS Canto II using the Diva software (BD Bioscience).

Cytokine assays

Peripheral blood was collected from mice treated with vehicle or 30 μg of rhGal-9 to assess cytokine production on the day following the administration of Gal-9 for 14 days. Serum cytokines were measured using a Bio-Plex™ Pro Mouse Cytokine Assay (BioRad Laboratories, Hercules, CA) according to the manufacturer's instructions.

Statistical analysis

Differences in aGVHD scores and serum cytokine levels between groups were determined using the Student's *t*-test. Differences in aGVHD histological scores were determined using the Mann–Whitney's *U*-test. Differences in survival among groups of mice were evaluated with a log-rank test of Kaplan–Meier survival curves. A p value of <0.05 was considered statistically significant.

Acknowledgements: This work was partly supported by Grant-in-Aids for Scientific Research and the Global COE Program "Center for Frontier Medicine" from the Ministry of Education, Culture, Sports, Science and Technology (MEXT) of Japan.

Conflict of interest: The authors declare no financial or commercial conflict of interest.

References

1 **Barondes, S. H., Castronovo, V., Cooper, D. N., Cummings, R. D., Drickamer, K., Feizi, T., Gitt, M. A. *et al.***, Galectins: a family of animal beta-galactoside-binding lectins. *Cell* 1994. **76**: 597–598.

2 **Cooper, D. N. and Barondes, S. H.**, God must love galectins; he made so many of them. *Glycobiology* 1999. **9**: 979–984.

3 **Chabot, S., Kashio, Y., Seki, M., Shirato, Y., Nakamura, K., Nishi, N., Nakamura, T. *et al.***, Regulation of galectin-9 expression and release in Jurkat T cell line cells. *Glycobiology* 2002. **12**: 111–118.

4 **Matsumoto, R., Matsumoto, H., Seki, M., Hata, M., Asano, Y., Kanegasaki, S., Stevens, R. L. and Hirashima, M.**, Human ecalectin, a variant of human galectin-9, is a novel eosinophil chemoattractant produced by T lymphocytes. *J. Biol. Chem.* 1998. **273**: 16976–16984.

5 **Kashio, Y., Nakamura, K., Abedin, M. J., Seki, M., Nishi, N., Yoshida, N., Nakamura, T. and Hirashima, M.**, Galectin-9 induces apoptosis through the calcium-calpain-caspase-1 pathway. *J. Immunol.* 2003. **170**: 3631–3636.

6 **Hirashima, M., Kashio, Y., Nishi, N., Yamauchi, A., Imaizumi, T. A., Kageshita, T., Saita, N. and Nakamura, T.**, Galectin-9 in physiological and pathological conditions. *Glycoconj. J.* 2004. **19**: 593–600.

7 **Irie, A., Yamauchi, A., Kontani, K., Kihara, M., Liu, D., Shirato, Y., Seki, M. *et al.***, Galectin-9 as a prognostic factor with antimetastatic potential in breast cancer. *Clin. Cancer Res.* 2005. **11**: 2962–2968.

8 **Kobayashi, T., Kuroda, J., Ashihara, E., Oomizu, S., Terui, Y., Taniyama, A., Adachi, S. *et al.***, Galectin-9 exhibits anti-myeloma activity through JNK and p38 MAP kinase pathways. *Leukemia* 2010. **24**: 843–850.

9 **Zhu, C., Anderson, A. C., Schubart, A., Xiong, H., Imitola, J., Khoury, S. J., Zheng, X. X. *et al.***, The Tim-3 ligand galectin-9 negatively regulates T helper type 1 immunity. *Nat. Immunol.* 2005. **6**: 1245–1252.

10 **Seki, M., Oomizu, S., Sakata, K. M., Sakata, A., Arikawa, T., Watanabe, K., Ito, K. *et al.***, Galectin-9 suppresses the generation of Th17, promotes the induction of regulatory T cells, and regulates experimental autoimmune arthritis. *Clin. Immunol.* 2008. **127**: 78–88.

11 **Wang, F., He, W., Zhou, H., Yuan, J., Wu, K., Xu, L. and Chen, Z. K.**, The Tim-3 ligand galectin-9 negatively regulates CD8+alloreactive T cell and prolongs survival of skin graft. *Cell Immunol.* 2007. **250**: 68–74.

12 **Hill, G. R., Crawford, J. M., Cooke, K. R., Brinson, Y. S., Pan, L. and Ferrara, J. L.**, Total body irradiation and acute graft-*versus*-host disease: the role of gastrointestinal damage and inflammatory cytokines. *Blood* 1997. **90**: 3204–3213.

13 **Hill, G. R., Cooke, K. R., Teshima, T., Crawford, J. M., Keith, J. C., Jr., Brinson, Y. S., Bungard, D. and Ferrara, J. L.**, Interleukin-11 promotes T cell polarization and prevents acute graft-versus-host disease after allogeneic bone marrow transplantation. *J. Clin. Invest.* 1998. **102**: 115–123.

14 **Hill, G. R. and Ferrara, J. L.**, The primacy of the gastrointestinal tract as a target organ of acute graft-*versus*-host disease: rationale for the use of cytokine shields in allogeneic bone marrow transplantation. *Blood* 2000. **95**: 2754–2759.

15 **Dai, S. Y., Nakagawa, R., Itoh, A., Murakami, H., Kashio, Y., Abe, H., Katoh, S. *et al.***, Galectin-9 induces maturation of human monocyte-derived dendritic cells. *J. Immunol.* 2005. **175**: 2974–2981.

16 **Anderson, A. C., Anderson, D. E., Bregoli, L., Hastings, W. D., Kassam, N., Lei, C., Chandwaskar, R. *et al.***, Promotion of tissue inflammation by the immune receptor Tim-3 expressed on innate immune cells. *Science* 2007. **318**: 1141–1143.

17 **Albert, M. H., Liu, Y., Anasetti, C. and Yu, X. Z.**, Antigen-dependent suppression of alloresponses by Foxp3-induced regulatory T cells in transplantation. *Eur. J. Immunol.* 2005. **35**: 2598–2607.

18 **Cohen, J. L. and Boyer, O.**, The role of CD4+CD25hi regulatory T cells in the physiopathogeny of graft-*versus*-host disease. *Curr. Opin. Immunol.* 2006. **18**: 580–585.

19 **Nguyen, V. H., Zeiser, R., Dasilva, D. L., Chang, D. S., Beilhack, A., Contag, C. H. and Negrin, R. S.**, In vivo dynamics of regulatory T-cell trafficking and survival predict effective strategies to control graft-*versus*-host disease following allogeneic transplantation. *Blood* 2007. **109**: 2649–2656.

20 **Harrington, L. E., Hatton, R. D., Mangan, P. R., Turner, H., Murphy, T. L., Murphy, K. M. and Weaver, C. T.**, Interleukin 17-producing CD4+effector T cells develop *via* a lineage distinct from the T helper type 1 and 2 lineages. *Nat. Immunol.* 2005. **6**: 1123–1132.

21 **Rohn, T. A., Jennings, G. T., Hernandez, M., Grest, P., Beck, M., Zou, Y., Kopf, M. and Bachmann, M. F.**, Vaccination against IL-17 suppresses autoimmune arthritis and encephalomyelitis. *Eur. J. Immunol.* 2006. **36**: 2857–2867.

22 **Hirota, K., Hashimoto, M., Yoshitomi, H., Tanaka, S., Nomura, T., Yamaguchi, T., Iwakura, Y. *et al.***, T cell self-reactivity forms a cytokine milieu for spontaneous development of IL-17+Th cells that cause autoimmune arthritis. *J. Exp. Med.* 2007. **204**: 41–47.

23 **Yi, T., Chen, Y., Wang, L., Du, G., Huang, D., Zhao, D., Johnston, H. *et al.***, Reciprocal differentiation and tissue-specific pathogenesis of Th1, Th2, and Th17 cells in graft-*versus*-host disease. *Blood* 2009. **114**: 3101–3112.

24 **Carlson, M. J., West, M. L., Coghill, J. M., Panoskaltsis-Mortari, A., Blazar, B. R. and Serody, J. S.**, In vitro-differentiated TH17 cells mediate lethal acute graft-*versus*-host disease with severe cutaneous and pulmonary pathologic manifestations. *Blood* 2009. **113**: 1365–1374.

25 **Kappel, L. W., Goldberg, G. L., King, C. G., Suh, D. Y., Smith, O. M., Ligh, C., Holland, A. M. *et al.***, IL-17 contributes to CD4-mediated graft-*versus*-host disease. *Blood* 2009. **113**: 945–952.

26 **Chen, Y., Langrish, C. L., McKenzie, B., Joyce-Shaikh, B., Stumhofer, J. S., McClanahan, T., Blumenschein, W. *et al.***, Anti-IL-23 therapy inhibits multiple inflammatory pathways and ameliorates autoimmune encephalomyelitis. *J. Clin. Invest.* 2006. **116**: 1317–1326.

27 **Nakae, S., Iwakura, Y., Suto, H. and Galli, S. J.**, Phenotypic differences between Th1 and Th17 cells and negative regulation of Th1 cell differentiation by IL-17. *J. Leukoc. Biol.* 2007. **81**: 1258–1268.

28 **Bettelli, E., Carrier, Y., Gao, W., Korn, T., Strom, T. B., Oukka, M., Weiner, H. L. and Kuchroo, V. K.**, Reciprocal developmental pathways for the generation of pathogenic effector TH17 and regulatory T cells. *Nature* 2006. **441**: 235–238.

29 **He, W., Fang, Z., Wang, F., Wu, K., Xu, Y., Zhou, H., Du, D. *et al.***, Galectin-9 significantly prolongs the survival of fully mismatched cardiac allografts in mice. *Transplantation* 2009. **88**: 782–790.

30 **Niwa, H., Yamamura, K. and Miyazaki, J.**, Efficient selection for high-expression transfectants with a novel eukaryotic vector. *Gene* 1991. **108**: 193–199.

31 **Okabe, M., Ikawa, M., Kominami, K., Nakanishi, T. and Nishimune, Y.**, 'Green mice' as a source of ubiquitous green cells. *FEBS Lett.* 1997. **407**: 313–319.

32 **Blanco, B., Perez-Simon, J. A., Sanchez-Abarca, L. I., Carvajal-Vergara, X., Mateos, J., Vidriales, B., Lopez-Holgado, N. *et al.***, Bortezomib induces selective depletion of alloreactive T lymphocytes and decreases the production of Th1 cytokines. *Blood* 2006. **107**: 3575–3583.

33 **Zhu, M., Wei, M. F., Liu, F., Shi, H. F. and Wang, G.**, Interleukin-10 modified dendritic cells induce allo-hyporesponsiveness and prolong small intestine allograft survival. *World J. Gastroenterol.* 2003. **9**: 2509–2512.

34 **Gerbitz, A., Ewing, P., Wilke, A., Schubert, T., Eissner, G., Dietl, B., Andreesen, R. *et al.***, Induction of heme oxygenase-1 before conditioning results in improved survival and reduced graft-*versus*-host disease after experimental allogeneic bone marrow transplantation. *Biol. Blood Marrow Transplant.* 2004. **10**: 461–472.

Abbreviations: **aGVHD:** acute GVH disease · **BMT:** BM transplantation · **Gal-9:** galectin-9 · **rh:** recombinant human · **TCD:** T-cell-depleted · **Tim-3:** T-cell immunoglobin domain and mucin domain-3

Full correspondence: Dr. Eishi Ashihara, Department of Transfusion Medicine and Cell Therapy, Kyoto University Hospital, 54 Kawahara-cho, Shogoin, Sakyo-ku, Kyoto 606-8507, Japan
Fax: +81-75-751-4283
e-mail: ash0325@kuhp.kyoto-u.ac.jp

Current address: Dr. Eishi Ashihara, Department of Molecular Cell Physiology, Kyoto Prefectural University of Medicine, 465 Kajii-cho, Kamigyo-ku, Kyoto 602-8566, Japan
Fax: +81-75-251-0295
e-mail: ash@koto.kpu-m.ac.jp

Received: 26/8/2010
Revised: 10/9/2010
Accepted: 29/10/2010
Accepted article online: 19/11/2010

Immunology Letters 135 (2011) 144–150

Contents lists available at ScienceDirect

Immunology Letters

journal homepage: www.elsevier.com/locate/immlet

Allograft inflammatory factor-1 is overexpressed and induces fibroblast chemotaxis in the skin of sclerodermatous GVHD in a murine model

Aihiro Yamamoto[a], Eishi Ashihara[b], Yoko Nakagawa[b], Hiroshi Obayashi[c], Mitsuhiro Ohta[d], Hirokazu Hara[e], Tetsuo Adachi[e], Takahiro Seno[a], Masatoshi Kadoya[a], Masahide Hamaguchi[a], Hidetaka Ishino[a], Masataka Kohno[a], Taira Maekawa[b], Yutaka Kawahito[a,*]

[a] Department of Inflammation and Immunology, Graduate School of Medical Science, Kyoto Prefectural University of Medicine, 465, Kajii-cho, Kawaramachi-Hirokoji, Kamigyo-ku, Kyoto 602-8566, Japan
[b] Department of Transfusion Medicine and Cell Therapy, Kyoto University Hospital, 54 Kawahara-cho, Shogoin, Sakyo-ku, Kyoto 606-8507, Japan
[c] Institute of Bio-Response Informatics, 22-15, Yousai, Momoyama-cho, Fushimi-ku, Kyoto 612-8016, Japan
[d] Department of Medical Biochemistry, Kobe Pharmaceutical University, 4-19-1, Motoyama-kita-machi, Higashinada-ku, Kobe 658-8558, Japan
[e] Department of Clinical Pharmaceutics, Gifu Pharmaceutical University, 1-25-4, Daigakunishi, Gifu 501-1196, Japan

ARTICLE INFO

Article history:
Received 19 August 2010
Received in revised form 23 October 2010
Accepted 24 October 2010
Available online 30 October 2010

Keywords:
Allograft inflammatory factor-1 (AIF-1)
GVHD
Scleroderma
Migration
Fibroblast

ABSTRACT

Allograft inflammatory factor (AIF)-1 has been identified in chronic rejection of rat cardiac allografts and is thought to be involved in the immune response. We previously showed that AIF-1 was strongly expressed in synovial tissues in rheumatoid arthritis and that rAIF-1 increased the IL-6 production of synoviocytes and peripheral blood mononuclear cells. Recently, the expression of AIF-1 has been reported in systemic sclerosis (SSc) tissues, whose clinical features and histopathology are similar to those of chronic graft-vs-host disease (GVHD). To clarify the pathogenic mechanism of fibrosis, we examined the expression and function of AIF in sclerodermatous (Scl) GVHD mice. We demonstrated that immunoreactive AIF-1 and IL-6 were significantly expressed in infiltrating mononuclear cells and fibroblasts in thickened skin of Scl GVHD mice compared with control. The immunohistochemical findings were confirmed by Western blot analysis. Wound healing assay also revealed that rAIF-1 increased the migration of normal human dermal fibroblasts (NHDF) directly, but cell growth assay did not show that rAIF-1 increased the proliferation of them. These findings suggest that AIF-1, which can induce the migration of fibroblasts and the production of IL-6 in affected skin tissues, is an important molecule promoting fibrosis in GVHD. Although the biological function of AIF-1 has not been completely elucidated, AIF-1 can induce IL-6 secretion on mononuclear cells and fibroblast chemotaxis. AIF-1 may accordingly provide an attractive new target for antifibrotic therapy in SSc as well as Scl GVHD.

1. Introduction

Allograft inflammatory factor (AIF)-1 is an IFN-γ-inducible, Ca^{2+}-binding EF-hand protein that is encoded within the HLA class III genomic region in the direct vicinity of TNF-α [1,2]. AIF-1 was originally identified and cloned from rat cardiac allografts undergoing chronic rejection [3]. AIF-1 expression has been documented in various human tissues and cells such as macrophage cell lines [4], peritoneal macrophages, spleen, peripheral blood leukocytes, and thymus [5], although its detailed physiological functions remain unclear. We previously proved that AIF-1 is strongly expressed in infiltrating mononuclear cells and synovial fibroblasts in rheumatoid arthritis (RA) compared with osteoarthritis (OA). In addition, AIF-1 induced the proliferation of cultured synovial cells in a dose-dependent manner and increased the IL-6 production of synoviocytes and peripheral blood mononuclear cells (PBMCs) [6]. Moreover, the expression of AIF-1 has been reported in systemic sclerosis (SSc) tissues [7]. The frequency of the AIF-1 rs2269475 TT genotype that results in a tryptophan to arginine amino acid substitution is significantly high in the patients with RA and SSc, and is associated with an increased risk of their development [8–10].

SSc is a chronic autoimmune disease characterized by fibrosis of skin and major organs such as lung, heart, gastrointestinal tract and widespread blood vessels. Progressive substitution of tissue structure by collagen-rich extra cellular matrix induces functional impairment of affected organs. The etiology is probably associated

Abbreviations: AIF-1, allograft inflammatory factor-1; BMT, bone marrow transplantation; GVHD, graft-vs-host disease; NHDF, normal human dermal fibroblasts; PDGF, platelet-derived growth factor; RA, rheumatoid arthritis; SSc, systemic sclerosis; Scl, sclerodermatous.

* Corresponding author. Tel.: +81 75 251 5505; fax: +81 75 252 3721.
E-mail address: kawahity@koto.kpu-m.ac.jp (Y. Kawahito).

0165-2478/$ – see front matter © 2010 Elsevier B.V. All rights reserved.
doi:10.1016/j.imlet.2010.10.015

with environmental and occupational exposure to organic solvents [11], genetic background, vascular damage, disorders of autoimmunity, collagen metabolism, cell growth factor and cytokines like connective tissue growth factor (CTGF) and TGF-β [12,13]. These factors are intricately intertwined and induce multiple clinical manifestations, but have not been elucidated in detail yet. In cells and tissues of various diseases including SSc, AIF-1 is expressed in T cells [14,15], macrophages, and endothelial cells [16,17] and may promote the expression of adhesion molecules that mediate specific homing into affected tissues [7]. Another recent study in vitro indicated that AIF-1 enhances the activation of T cells, which increase chemotaxis and induces a profibrotic phenotype [15,14], but the T cells are forcedly transfected with the vector expressing AIF-1. Thus, AIF-1 is thought to play a fundamental role in several cell types involved in chronic immunological inflammatory processes.

SSc resembles graft-vs-host disease (GVHD) both in its clinical features and histopathology [18]. For example, chronic GVHD has SSc like clinical features such as a skin fibrosis. Investigation of the fibrosing process in GVHD may help to elucidate the pathogenesis of fibrosis in SSc as well. The occurrence and extent of tissue fibrosis are thought to be influenced by minor histocompatibility mismatches and radiation exposure before transplant. These factors cause various immune responses of graft failure in bone marrow transplantation [19,20], but the detailed mechanism of fibrosis is still unclear. The phenotypic features in Scl GVHD get expressed about 3 weeks after transplant and are characterized by loss of dermal fat, thickening of skin, infiltration of numerous mononuclear cells and fibroblasts, and acceleration of collagen synthesis [19,21]. Clarification of the immunological mechanisms underlying skin fibrosis in GVHD will also shed light on the pathogenesis of SSc. However, no reports are available on the involvement of AIF-1 in GVHD. Furthermore, the pathophysiologic significance of AIF-1 in skin fibrosis has not been elucidated. This prompted us to examine the expression of AIF-1 and its function in fibrosis by using this Scl GVHD model [19] that recapitulates important features of SSc.

2. Materials and methods

2.1. Bone marrow transplantation

Six to 8-week-old male B10.D2 mice (H-2^d, Oriental Bio Service) were used as donors and 6–8-week-old female BALB/c mice (H-2^d, SRL) as recipients, for bone marrow transplantation to Scl GVHD with a standard method using spleen cells as the source of mature T cells. BALB/c mice were irradiated with 7.5 Gy. About 6 h later, recipient mice were injected via the tail vein with male donor bone marrow (4×10^6/mouse) and spleen cells (1×10^7/mouse) suspended in PBS. The control group consisted of female BALB/c recipient mice that received male B10.D2 bone marrow cells, namely a T cell depleted-bone marrow transplantation (TCD-BMT) group. Transplanted mice were maintained in sterile cages and supplied with autoclaved food. We performed the experiments five times, with five animals per group (Scl GVHD or TCD-BMT) examined in each experiment. Approval for these studies was obtained from the Committee on Animal Research of the Kyoto University Faculty of Medicine.

2.2. Collection of tissue and preparation of normal human dermal fibroblasts

Allogeneic BMT mice had significantly lower body weights than TCD-BMT mice from day 10 after BMT and extensive thickened skin (data not shown). Five transplanted animals per group were sacrificed by cervical dislocation on day 21 after BMT. Day 21 after BMT was chosen because it is the earliest time point when Scl GVHD reliably develops in mice receiving allogeneic BMT. Skin was depilated and harvested for immunostaining and Western blotting. Normal human dermal fibroblasts (NHDF) were obtained from Sanko Junyaku Co., Ltd [22,23] and cultured in fibroblast basal medium with human fibroblast growth factor-B (1 μg/ml), insulin (5 mg/ml), 0.1% gentamicin/amphotericin-B, and 10% fetal bovine serum in a humidified incubator at 37 °C in the presence of 5% CO_2. We actually used NHDF after three or four passages in cell culture.

2.3. Peptide synthesis and preparation of anti-human AIF-1_{53-71} and AIF-$1_{113-129}$ Abs

Two synthetic peptides, which corresponded to residues 53–71 and 113–129 of human AIF-1 (AIF-1_{53-71} and AIF-$1_{113-129}$, respectively) as deduced from the nucleotide sequence of the human AIF-1 gene, were obtained with an additional cysteine residue at the N terminus (Biologica). Following purification by reversed phase HPLC, the synthetic peptide (purity >90%) was coupled to keyhole limpet hemocyanin with N-(ε-maleimidocaproyloxy) succinimide (Sigma–Aldrich). The carrier-conjugated peptide was then emulsified with Freund's complete adjuvant (Difco Laboratories) and injected s.c. (0.5 mg/injection) into rabbits. The rabbits were immunized six times at 10-day intervals. Blood samples were collected 10 days after the last injection, and the specific Ab in the sera was purified using an AIF-1 peptide-coupled cyanogen bromide-activated Sepharose affinity column. The Abs reacted with protein from abdominal adipose tissue and PBMC that is identical to the molecular size of purified recombinant human AIF-1.

2.4. Expression of rAIF-1 and preparation of anti-rAIF-1 Ab

Human AIF-1 cDNA was amplified from human peripheral lymphocyte cDNA (BD Clontech, California, USA) using PCR. The forward and reverse primers were 5′ -GTG GAT CCA TGA GCC AAA CCA GGG ATT T-3′ (containing *Bam*HI site) and 5′-CAC TCG AGT CAG ATA GGG CTT TCT TGG CT-3′ (containing *Xho*I site), respectively. To express AIF-1 as a GST fusion protein, the DNA fragment obtained was inserted in the *Bam*HI/*Xho*I sites of pGEX-4 (Amersham Biosciences) in frame. The fusion protein was purified with a GST purification system (Amersham Biosciences) and affinity chromatography with anti-AIF-$1_{113-129}$ Ab. To investigate the effect of AIF-1 on the cell proliferation and cytokine induction, rAIF-1 was treated with detoxi-gel endotoxin removing gel (Pierce). Endotoxin detection was performed using *Limulus* amoebocyte lysate analysis (Wako Pure Chemical), and treated AIF protein was confirmed to contain <0.1 ng/μg of endotoxin. AIF protein we synthesized was named AIF-5 according to a new nomenclature of the AIF family of proteins [24]. This AIF splice variants IRT-1, G1, BART-1 are encoded in the same region of the BAT2 gene on chromosome 6 [5]. Anti-rAIF-1 antiserum was raised in a similar manner as anti-synthetic peptide Ab by injecting 50 mg of human rAIF-1 into a rabbit. The human rAIF-1 Ab IgG fraction was prepared by chromatography on a human rAIF-1-coupled cyanogen bromide-activated Sepharose affinity column and biotinylated with 5-(N-succinimidyloxycarbonyl)pentyl D-biotinamide (Dojindo Chemical).

2.5. Immunohistochemical analysis of AIF-1 expression in skin

Immunohistochemical staining was performed using the avidin–biotin peroxidase complex system. Skin tissue specimens were preserved in 10% buffered formalin and embedded in paraf-

fin. Specimens were serially sectioned onto microscope slides at a thickness of 4 μm and then deparaffinized. Tissue sections were immersed for 45 min in 0.3% peroxide in methanol to block endogenous peroxidase activity. Nonspecific binding sites were saturated by exposure to 0.2% BSA and normal goat serum diluted 1/66.7 in PBS (pH 7.4) for 20 min. Primary Abs against human AIF-$1_{113-129}$ (1/800 dilution in PBS), IL-6 (1/50 dilution in PBS) (Santa Cruz), collagen I (1/200 dilution in PBS) (Abcam) and control normal rabbit serum (Dako) were applied to tissue sections and incubated overnight at 4 °C. The slides were then washed with PBS for 10 min. Biotinylated goat anti-rabbit IgG (Vector Laboratories) in 10 ml of PBS was applied to tissue sections, and the slides were incubated at room temperature for 30 min. They were then washed with PBS for 10 min, followed by incubation with prepared avidin DH-biotinylated peroxidase complex (Vector Laboratories) for 45 min. After washing with PBS for 10 min, color was developed by immersing the sections in peroxidase substrate solution containing 0.05% (w/v) 3,3′-diaminobenzidine tetrahydorochloride (Vector Laboratories) and 0.01% H_2O_2 in 0.05 mol/L Tris-buffered saline (pH 7.2) for 5 min. Positive staining was indicated by brownish black deposits, and counterstaining was performed with hematoxylin. Specific Ab staining was always compared with corresponding isotype control-stained sections on the same slide.

For each of the tissue specimens from Scl GVHD and TCD-BMT mice, the extent and intensity of staining with anti-AIF-$1_{113-129}$, IL-6, and collagen I Abs in mononuclear cells and fibroblasts in the skin were graded on a scale of 0–3+ by two blinded observers on two separate occasions using coded slides as previously described [6]. A 3+ grade implies maximally intense staining, whereas 0 implies no staining.

2.6. Western blot analysis

Western blot analysis was performed as previously described [25]. Briefly, skin specimens were homogenized on ice by sonication and solubilized in lysis buffer (PBS, pH 7.4, containing 1% Nonidet P-40, 0.5% sodium deoxycholate, 0.1% SDS, and 0.6 mM PMSF). Thirty micrograms of each total protein extract from skin tissues were electrophorised in 4–20% gradient gel SDS-PAGE. Following electrotransfer to a polyvinylidine difluoride membrane. The membranes were saturated with 5% (wt/vol) nonfat dry milk in TBST (25 mM Tris [tris(hydroxymethyl)aminomethane]–HCl, pH 7.8, 140 mM NaCl, 0.1% [vol/vol] Tween 20) and then incubated overnight with anti-rAIF-1 Ab (1/500 diluted by Can Get Signal [26,27]; Toyobo Life Science) and anti-IL-6 Ab (Santa Cruz; 1/500 dilution). The membranes were washed thoroughly with TBST and incubated with an HRP-linked anti-rabbit IgG (Amersham Biosciences, 1/1000 diluted with Can Get Signal) for 1 h. After washing, immunoreactivity was detected by ECL using ECL Plus Western blotting detection reagents (Amersham Biosciences). Images were obtained by exposure to Hyperfilm (Amersham Pharmacia Biotech) for 5 min.

2.7. Wound healing assay

NHDF were seeded in 92 mm dishes at a concentration of 3×10^5 cells/dish in a volume of 10 ml of Fibroblast Cell Medium (Sanko Junyaku Co., Ltd) consisting of Fibroblast Cell Basal Medium and the following growth supplements: human fibroblast growth factor-B, 0.5 ml; insulin, 0.5 ml; FBS, 10 ml; GA-1000, 0.5 ml and cultured to confluence. Confluent monolayer NHDF in these dishes were scratched with 200 μl tip (0 h), and then cultured [28] in the presence of 0.2% FBS in combination with 100 ng/ml of Lipopolysaccharide (LPS) or 1–100 ng/ml of AIF-1 with or without anti-AIF-1 Ab for 24 h. At 0 h and 24 h, the scratched monolayer cultures were photographed using an inverted microscope. Quantification was done by measuring the number of pixels in each wound closure area using Adobe Photoshop [28]. Data are expressed as percentage wound closure relative to the wound closure area in the control medium.

2.8. Cell growth assay

To evaluate the effect of AIF-1 on cell growth of NHDF, NHDF were inoculated into 96 well plates (1.5×10^3 cells/well) and incubated in Fibroblast Cell Medium. Twenty-four hours later, the medium were changed to in the presence of 0.2% FBS in combination with 100 ng/ml of LPS or 1-100 ng/ml of AIF-1 with or without anti-AIF-1 Ab for 72 h. The medium of positive control group remained as it was for following 72 h. Then the cell viability was estimated by WST-1 assay (Takara Bio Inc.) by measuring the absorbance at 450 nm in multiwell plate reader EMax (Molecular Devices, Japan). Each measurement was determined in six separate experiments, and the results are presented as a percentage of the value for the control cultures.

2.9. ELISA

We measured IL-6 and platelet-derived growth factor (PDGF) in the supernatant of cultured NHDF stimulated by LPS or various concentrations of AIF-1 with or without anti-AIF-1 Ab using commercial ELISA kits (IL-6 ELISA kit; eBioscience, PDGF ELISA kit; R&D Systems) according to the manufacturer's instructions. The supernatant used in the experiments was the same as that obtained at the wound healing assay (details described in the paragraph on the wound healing assay). In brief, microtiter plates (Corning Costar 9018) were coated with pre-titrated capture Ab overnight at 4 °C. After washing, nonspecific binding sites in each well were blocked with assay diluent included in each kit. Standard solution (4–500 pg/ml) and supernatant samples were added to the wells, and the plate was incubated at room temperature for 1 h. After washing, pre-titrated avidin-HRP was added to each well and incubated at room temperature for 30 min. After final washing, substrate solution was added to each well and allowed to react at room temperature for 15 min. The reaction was stopped by the addition of 1 M phosphoric acid, after which OD values at 450 nm were read with an ELISA plate reader. The detection limit of the assay was 4 pg/ml.

2.10. Statistical analysis

We conducted experiments to reveal the cutaneous cytokine expression in murine Scl GVHD five times. Five mice per group and per time point were examined. The results from Scl GVHD mice were compared each time with those from TCD-BMT mice according to the same protocols of irradiation and transplantation. The graded scores of the extent and intensity of immunostaining with anti-AIF-1 and IL-6 Ab between Scl GVHD and TCD-BMT groups were analyzed by the Mann–Whitney U test. We repeated each in vitro experiment five times. Differences in induction of IL-6 in the cultured NHDF supernatant after rAIF-1 stimulation between the six groups were analyzed by ANOVA followed by Bonferroni/Dunn's multiple comparison test. The results of the percentage wound closure of NHDF and WST-1 assay were also analyzed by ANOVA followed by Bonferroni/Dunn's multiple comparison test. $p < 0.05$ was considered significantly different.

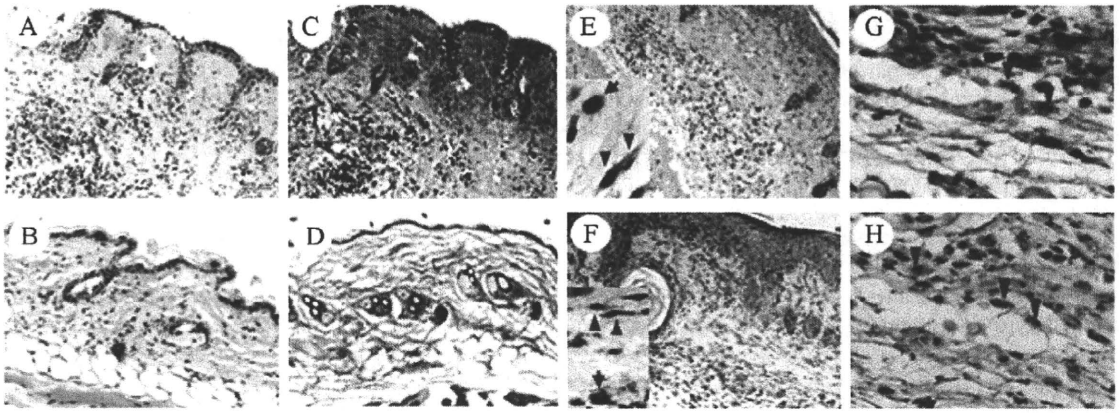

Fig. 1. Histopathological analysis of BMT skin tissues. (A, C, E–H) Skin tissue from Scl GVHD murine skin ($n = 5$), (B, D) Skin tissue from TCD-BMT murine skin ($n = 5$). (A, B) HE staining. (C, D) Masson Trichrome staining. (E, F) Immunostaining with anti-AIF-1 Ab and anti-IL-6 Ab, respectively. (G, H) Fibroblasts are stained by AIF-1 and collagen I, respectively. Fibroblasts stained by anti-collagen I Ab have morphologically branched or demonstrate a spindle shaped cytoplasm with an elliptical nucleus (arrowhead). Mononuclear cells are mostly round with round nuclei (arrow). The same fibroblasts were stained both in sequential paraffin slices. (A–D) magnification ×40. (E, F) magnification ×40 and ×400. (G, H) magnification ×400.

3. Results

3.1. Immunohistochemical analysis of Scl GVHD murine skin

Allogeneic BMT mice had significantly lower body weights than TCD-BMT mice from day 10 after BMT (data not shown). We demonstrated the extent of thickened skin in these mice histologically. On day 21 after BMT, at an early stage of GVHD with hair loss, Scl GVHD mice showed a mixture of large pale oval numerous mononuclear cells and spindle shaped fibroblasts that infiltrated thickened skin compared with TCD-BMT mice (Fig. 1A and B). Fibrosis of the thickened dermal layer was also stained blue by Masson Trichrome (Fig. 1C and D). Spindle shaped cells of the thickened dermal layer were stained by anti-collagen I Ab. These fibroblasts also expressed AIF-1 in serial sections (Fig. 1E, G and H). Moreover, we found significantly enhanced expression of AIF-1 in infiltrating mononuclear cells and fibroblasts (histopathological score; mean ± SE, 2.83 ± 0.17) in Scl GVHD murine skin tissues. In contrast, the level of AIF-1 expression in infiltrating mononuclear cells and fibroblasts was low (histopathological score; mean ± SE, 0.58 ± 0.10) in TCD-BMT murine skin tissues (Fig. 2A). We also found significant expression of IL-6 in these cells of Scl GVHD skin (histopathological score; mean ± SE, 2.58 ± 0.17) compared with TCD-BMT skin (histopathological score; mean ± SE, 0.58 ± 0.10) (Figs. 1F and 2B). Immunostaining of tissue sections with normal rabbit serum was completely negative in all skin tissues (data not shown).

As seen in Fig. 3, Western blot analysis detected AIF-1 protein at 17 kDa as a single band in protein extracts from skin tissues of Scl GVHD, TCD-BMT, and normal mice. The intensity of AIF-1 protein band was greatly enhanced in the skin of Scl GVHD mice compared with that in TCD-BMT (Fig. 3A) and normal mice (data not shown). The IL-6 detected at 28 kDa, was also more highly expressed in Scl GVHD mice than in TCD-BMT mice (Fig. 3B) and normal mice (data not shown).

3.2. IL-6 secretion from NHDF by rAIF-1 stimulation

The IL-6 and PDGF in the supernatant from cultured NHDF after rAIF-1 stimulation for 24 h were slightly elevated in spite of the dose of rAIF-1, but the increase in the IL-6 concentration induced by 100 ng/ml rAIF-1 stimulation was more significant than that by 1 ng/ml or 10 ng/ml rAIF-1stimulation (Fig. 4).

3.3. Migration and proliferation of dermal fibroblasts following rAIF-1 stimulation

We examined the effect of AIF-1 upon the cell migration and proliferation of normal human dermal fibroblasts (NHDF) by quantifying the wound closure area in a wound healing assay. Confluent monolayers of NHDF were scratched to form wound and cultured in the absence or presence of rAIF-1 or anti-AIF-1 Ab for 24 h. rAIF-1 resulted in the increased cell migration in a dose-dependent manner and induced a significant increase in these parameters as compared with the control (Fig. 5A and B). The effect of 100 ng/ml of rAIF-1 was similar to that of 100 ng/ml of LPS. In WST-1 assay, the cell proliferation of NHDF stimulated by rAIF-1 did not induce a significant increase compared with the positive control (Fibroblast Cell Medium) (data not shown). These findings indicate that rAIF-1 induce the migration of dermal fibroblast but not proliferation.

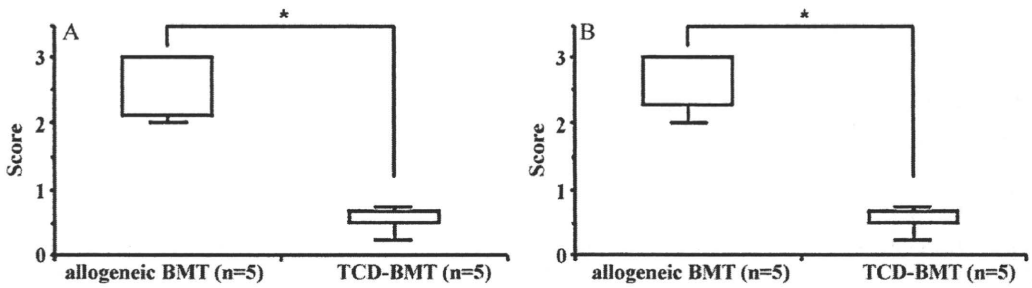

Fig. 2. Histopathological scores of immunoreactive AIF-1 and IL-6 in BMT skin tissues. A and B indicate the histopathological graded scores of the extent and intensity of immunostaining with anti-AIF-1 Ab and anti-IL-6 Ab, respectively, for allogeneic BMT skin tissues ($n = 5$) and TCD-BMT skin tissues ($n = 5$). The box plot includes an interquartile range (box), whereas the whiskers represent the 10–90th percentiles. The differences between two groups were analyzed by the Mann–Whitney U test. $^*p < 0.01$.